AD-A079 661 TEXAS UNIV AT AUSTIN APPLIED RESEARCH LABS F/G 20/1
THE EFFECT OF SEDIMENT RIGIDITY ON BOTTOM REFLECTION LOSS.(U)
SEP 79 P J VIDMAR N00014-78-C-0113
UNCLASSIFIED ARL-TR-79-49 NL

1 OF 2
AD A 079661

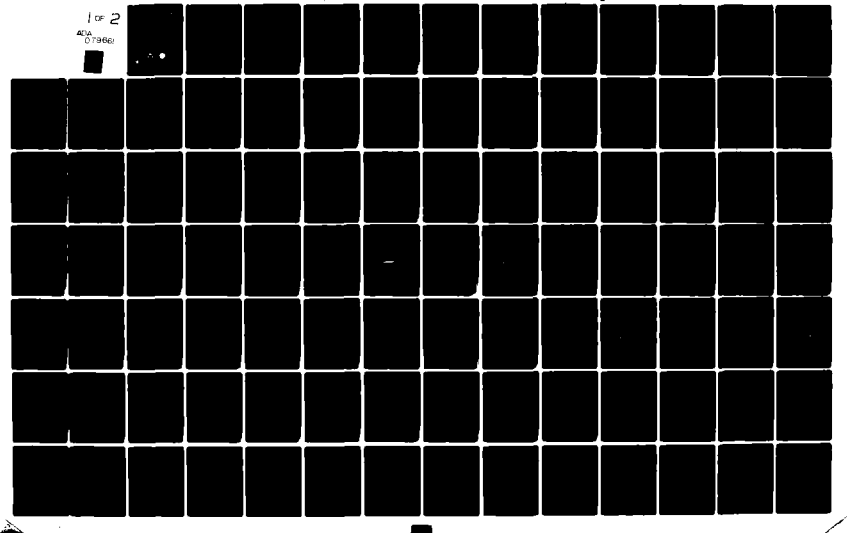

ARL-TR-79-49

THE EFFECT OF SEDIMENT RIGIDITY ON BOTTOM REFLECTION LOSS

Paul J. Vidmar

APPLIED RESEARCH LABORATORIES
THE UNIVERSITY OF TEXAS AT AUSTIN
POST OFFICE BOX 8029, AUSTIN, TEXAS 78712

19 September 1979

Technical Report

Prepared for:

NAVAL OCEAN RESEARCH AND DEVELOPMENT ACTIVITY
NSTL STATION, MS 39529

UNCLASSIFIED

SECURITY CLASSIFICATION OF THIS PAGE *(When Data Entered)*

REPORT DOCUMENTATION PAGE

READ INSTRUCTIONS BEFORE COMPLETING FORM

1. REPORT NUMBER
2. GOVT ACCESSION NO.
3. RECIPIENT'S CATALOG NUMBER

4. TITLE *(and Subtitle)*: THE EFFECT OF SEDIMENT RIGIDITY ON BOTTOM REFLECTION LOSS

5. TYPE OF REPORT & PERIOD COVERED: technical report

6. PERFORMING ORG. REPORT NUMBER: ARL-TR-79-49

7. AUTHOR(s): Paul J. Vidmar

8. CONTRACT OR GRANT NUMBER(s): N00014-78-C-0113

9. PERFORMING ORGANIZATION NAME AND ADDRESS
Applied Research Laboratories
The University of Texas at Austin
Austin, Texas 78712

10. PROGRAM ELEMENT, PROJECT, TASK AREA & WORK UNIT NUMBERS

11. CONTROLLING OFFICE NAME AND ADDRESS
Naval Ocean Research and Development Activity
NSTL Station, MS 39529

12. REPORT DATE: 19 Sep 1979

13. NUMBER OF PAGES: 100

14. MONITORING AGENCY NAME & ADDRESS *(if different from Controlling Office)*
Naval Electronic Systems Command
Department of the Navy
Washington, DC 20360

12 105

15. SECURITY CLASS. *(of this report)*: UNCLASSIFIED

15a. DECLASSIFICATION DOWNGRADING SCHEDULE: N/A

16. DISTRIBUTION STATEMENT *(of this Report)*

Approved for public release; distribution unlimited.

17. DISTRIBUTION STATEMENT *(of the abstract entered in Block 20, if different from Report)*

18. SUPPLEMENTARY NOTES

19. KEY WORDS *(Continue on reverse side if necessary and identify by block number)*

404 434

20. ABSTRACT *(Continue on reverse side if necessary and identify by block number)*

The plane wave reflection coefficient R of a horizontally stratified ocean bottom is studied for typical deep sea sediment types in order to determine the importance of sediment rigidity (shear wave propagation) on bottom reflection loss, RL = $-20 \log_{10}(|R|)$ dB. The emphasis is on, but not restricted to, low grazing angles (0 to 45°) and low frequencies (10 to 200 Hz). R is studied using a computational model accurate for frequencies above 10 Hz which treats a single inhomogeneous (solid) sediment

DD FORM 1 JAN 73 1473 EDITION OF 1 NOV 65 IS OBSOLETE

RL = −20 log (absolute value of R) dB

UNCLASSIFIED

SECURITY CLASSIFICATION OF THIS PAGE *(When Data Entered)*

20a. Cont'd.

layer overlying a homogeneous (solid) substrate. Comparing RL due to a solid sediment RLS with RL of a fluid sediment RLF yields $\Delta RL = RLS - RLF$, the change in RL produced by sediment rigidity.

For a hypothetical turbidite layer the dependence of ΔRL on layer thickness suggests an empirical classification of sediments into "thick" and "thin" categories. For a thick (500 m) layer $\Delta RL \sim 0$ at low grazing angles and sediment rigidity can be neglected. For a thin (36 m) layer at a grazing angle of 20°, $\Delta RL \sim 20$ dB at 20 Hz and $\Delta RL \approx 4$ dB at 200 Hz; sediment rigidity in this case is not negligible but produces significant increases in reflection loss.

The frequency dependence of RLS for the 36 m thick layer reveals high and low frequency regimes with strikingly different behavior. For a grazing angle of 20°, ΔRL is about 2 dB at low frequencies with very large peaks (~25 dB) occurring at 2 Hz intervals. These peaks are the result of interference effects related to sediment shear wave propagation. The interference peaks decrease in magnitude at higher frequencies as shear wave attenuation increases and reduces the magnitude of interference effects. At high frequencies the peaks have entirely disappeared. A value of $\Delta RL \sim 4$ dB persists and there is also a gentle oscillation occurring in both RLS and RLF due to sediment compressional wave interference effects.

An examination of the reflection and transmission coefficients at the water-sediment and sediment-substrate interfaces, by means of an expansion in the ratio of sediment shear speed to the sound speed in water, reveals the mechanism for exciting sediment shear waves and provides an understanding of the empirical separation into "thick" and "thin" sediments. At the water-sediment interface sediment shear waves are not efficiently excited and the sediment can be treated, in most cases, as a fluid. The dominant mechanism for exciting sediment shear waves is compressional wave conversion at the sediment-substrate interface. At a given grazing angle in a thick sediment the compressional wave will have a turning point well above the sediment-substrate. Compressional wave amplitude at the interface will be small. As a result very little energy is transferred to sediment shear waves, and the sediment can be accurately described as a fluid. For a thin sediment the compressional wave strikes the interface or has its turning point near the interface; compressional wave amplitude at the interface is significant, sediment shear waves are excited, and the sediment must be treated as a solid. The difference between a "thick" and a "thin" layer is then translated into a question of whether the compressional wave significantly interacts (thin) with the substrate or not (thick).

Parameter studies are reported which investigate the dependence of RLS on bottom parameters and gradients. Homogeneous sediment layers and layers with gradients are studied to determine which parameters are important in describing the acoustic properties of solid sediments. Variations about a parameter set indicate the accuracy needed in specifying bottom parameters to accurately predict reflection loss.

This work has been supported by Naval Ocean Research and Development Activity and Naval Electronic Systems Command.

TABLE OF CONTENTS

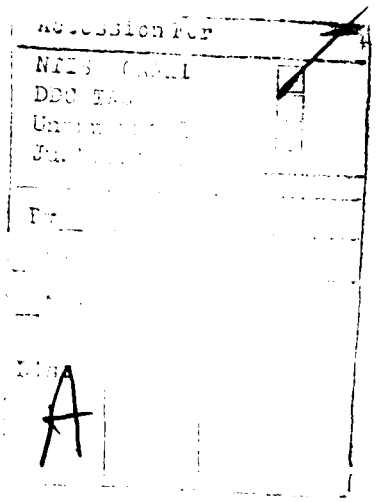

LIST OF FIGURES

LIST OF TABLES

I. INTRODUCTION

Acoustic interaction with the ocean bottom is an important factor in determining the propagation of low frequency sound waves in the ocean. Because of the long wavelengths involved, the acoustic energy penetrates into the ocean bottom and interacts with the subbottom structure. The excitation of compressional (P), shear (S), and interface waves in the sediment-substrate structure are important energy loss processes affecting the propagation of low frequency sound, particularly when compared to the negligible attenuation occurring within the water column itself.

Determining the dependence of the plane wave reflection coefficient R (and its analog, the reflection loss RL = $-20 \log_{10}(|R|)$) on subbottom parameters is a useful and traditional method of studying the bottom interaction. Parameter studies of R, using computational models of the bottom interaction for an assumed fluid sediment, have determined the importance of several subbottom features. Density gradients have been found to be negligible in typical deep sea sediments.[1] The effect of P wave speed[2,3] and absorption profiles[4] have been treated. Interface wave excitation at the sediment-substrate interface has been identified as a loss mechanism.[5,6] The effect of surface roughness at the water-sediment interface has also been studied.[7]

The effect of sediment rigidity (shear wave propagation) on R has received little attention and is not well understood. Although included in some computational models,[8,9] no systematic studies have been made to determine the importance of sediment S wave propagation. A detailed study at this time would provide realistic and useful results since parameter ranges can now be constrained by recently available estimates of sediment S wave properties.[10,11] Such a study is of importance since the relatively high attenuation of sediment S waves makes their excitation a potentially important energy loss mechanism. Recent work[13,14] indicates that sediment

S wave excitation, while negligible in thick sediment layers, can be the dominant energy loss mechanism in thin sediment layers.

In this paper we present the results of our investigation of the effect of sediment rigidity on R. Our emphasis is on, but not restricted to, low grazing angles and typical deep sea sediment types. Our study shows that the mechanism for sediment S wave excitation is primarily P wave conversion at the sediment-substrate interface. (The gradient-driven P-S conversion is negligible for these sediment types for frequencies above about 3 Hz.[15]) An examination of the reflection and transmission coefficients shows that this is due to the small surficial shear wave speed in the sediment. Typical deep sea sediments can be accurately treated as fluids at the water-sediment interface where sediment S wave excitation is negligible. This excitation mechanism also allows a classification of sediment layers into "thick" and "thin" categories. For a thick sediment the P wave has its turning point well above the sediment-substrate interface. Consequently, sediment S wave excitation is negligible and the sediment can be accurately treated as a fluid. For a thin sediment the P wave significantly interacts with the substrate. Shear waves are excited in the sediment, and the sediment must be treated as a solid. For thin sediments our study shows low and high frequency regimes with strikingly different behavior. At low frequencies sediment shear wave attenuation is small, and interference effects due to propagation of S waves within the sediment column dominate the dependence of R on frequency. Large (>20 dB) peaks in RL occur. The frequency separation between these peaks is related to changes in S wave phase of 2π. At higher frequencies the increased shear wave attenuation destroys this peak structure. The shear waves excited at the sediment-substrate interface are then totally absorbed within the sediment, resulting in an almost constant additional loss (~4 dB) compared to the RL of a fluid sediment. We also present parameter studies aimed at identifying important parameters in solid sediments and the accuracy to which these parameters must be known to accurately compute RL.

The tool used in this study is a recently developed computational model[15] of R which allows sediment shear wave propagation. The model assumes horizontal stratification and treats a single sediment layer overlying a semiinfinite homogeneous substrate. The model is based on numerical integration of the depth separated wave equations for the potentials giving rise to the compressional and shear waves in the sediment, and thus includes all wave properties, such as penetration beyond turning points, boundary wave excitation, et The use of numerical integration permits sediment parameters to have arbitrary depth dependencies and to be individually varied to determine their influence on R. The basic approximation of the model is the use of the Helmholtz equations with depth dependent wave number to describe the potentials. This is essentially a high frequency approximation in which effects directly dependent on gradients and the continuous coupling between shear and compressional waves are neglected. For parameters typical of deep sea sediments, this model is accurate for frequencies above about 10 Hz.

The first section of this paper discusses a hypothetical turbidite layer with realistic parameters and depth variations. By varying the sediment layer thickness and the wave frequency, our basic results are observed. The second section develops a theory of the reflection and transmission coefficients based on an expansion in the sediment S wave velocity. These are used to construct a ray picture of the acoustic interaction, which is then used to interpret the results of the hypothetical turbidite layer study. The wave theory model verifies some parameter dependencies predicted by the ray model. The next section presents the results of parameter studies for homogeneous layers and layers with gradients. The parameters of a realistic layer are perturbed to obtain an estimate of the accuracy required in the values of these parameters to compute R accurately. The effect of sediment rigidity on interface wave excitation is also treated. The final section summarizes the results of our study.

II. HYPOTHETICAL TURBIDITE LAYER

In this section we consider the effect of sediment rigidity on the reflection loss from a hypothetical turbidite layer. RL is studied as a function of grazing angle θ, frequency f, and sediment layer thickness H (the grazing angle is the complement of the angle of incidence γ, i.e., $\theta=90-\gamma$). Our results agree with the recent work of Fryer[9] for a thick sediment layer and illustrate our most important results for thin sediment layers.

The depth structure of the turbidite layer is given in Table I. These parameters were obtained from the recent work of Fryer.[9] Constant gradients are assumed between the depths given in Table I, the parameter values are representative of this type of sediment, and the attenuation is assumed to depend linearly on frequency. Fryer's 650 m sediment layer was truncated at 518 m so that our numerical model would produce accurate results at low grazing angles for a frequency of 20 Hz. For a significantly thicker layer (650 m) the S wave attenuation and the exponential behavior of the P wave potential combine with the finite computer word length to produce a loss of precision for grazing angles below about 20°. The accuracy of the calculated RL at 518 m was established in two ways. First, for a solid sediment, RL below $\theta=25°$ agrees to within 0.1% for H = 518 m, 385 m, and 252 m. Second, for the same thicknesses and grazing angles, RL for both fluid and solid sediment structure agreed to within 1%. The theoretical analysis of the next section of this report shows that this constancy of RL with depth at low grazing angles and the lack of dependence on sediment rigidity are expected for these relatively thick sediments. Since it is less and less difficult to maintain precision as H decreases, the accuracy of the computation at 518 m is verified.

TABLE I

ACOUSTIC PARAMETERS OF THE HYPOTHETICAL TURBIDITE LAYER

c is the compressional wave speed;
v is the shear wave speed;
ρ is the density;
k_p is the compressional wave attenuation;
k_s is the shear wave attenuation.

Depth (m)	c (m/sec)	k_p (dB/m/kHz)	ρ (g/cm^3)	v (m/sec)	k_s (dB/m/kHz)
Water	1530	--	1.030	--	--
0	1510	0.065	1.530	116	8.46
36	1582	0.100	1.579	283	5.60
120	1674	0.200	1.689	391	8.60
518	1992	0.135	2.010	621	4.35
Substrate	4460	0.008	2.460	2400	0.04

Figure 1 shows RL as a function of θ for f = 20 Hz and H = 518 m. The three curves were obtained for different sediment-substrate configurations. The dotted line was obtained for a fluid sediment and fluid substrate (the FF case), the dashed line for a fluid sediment and solid substrate (the FS case), and the solid line for a solid sediment and solid substrate (the SS case). The remaining case of a solid sediment and a fluid substrate (the SF case) is not shown in Fig. 1. It is essentially identical to the FF case over the entire range of grazing angles, frequencies, and sediment thicknesses considered. The parameters for the fluid sediment and fluid substrate were obtained from Table I by ignoring the S wave parameters.

Comparing the curves of Fig. 1 shows the effect of sediment rigidity in this thick layer. Case FF has the expected small RL for small θ followed by an oscillatory structure due to interference between the wave directly reflected from the water-sediment interface and the P wave penetrating the sediment and returning to the water. Beyond the critical angle for substrate P wave propagation ($\theta_p \simeq 70°$), RL increases as energy is carried away by substrate P waves. Comparing the FS and FF cases shows the effect of substrate rigidity. At both small and large grazing angles the FS and FF cases are nearly identical, an indication that substrate rigidity has a negligible effect at these angles. RL, however, increases between the critical angle for substrate S wave propagation θ_s and θ_p. Substrate S waves carry away additional energy in this angular range. Comparing the SS and FS cases shows the effect of sediment rigidity alone. Except for grazing angles between θ_s and θ_p, sediment S wave propagation has a negligible effect on RL. The major effect between the critical angles is a shift in the peak structure.

Comparison of Fig. 1 with Fryer's Fig. 8 shows qualitative agreement between the corresponding FF and SS cases. Fryer obtained his result using a different computational technique and for a thicker (650 m) sediment layer. The conclusion can be drawn from our intermediate FS

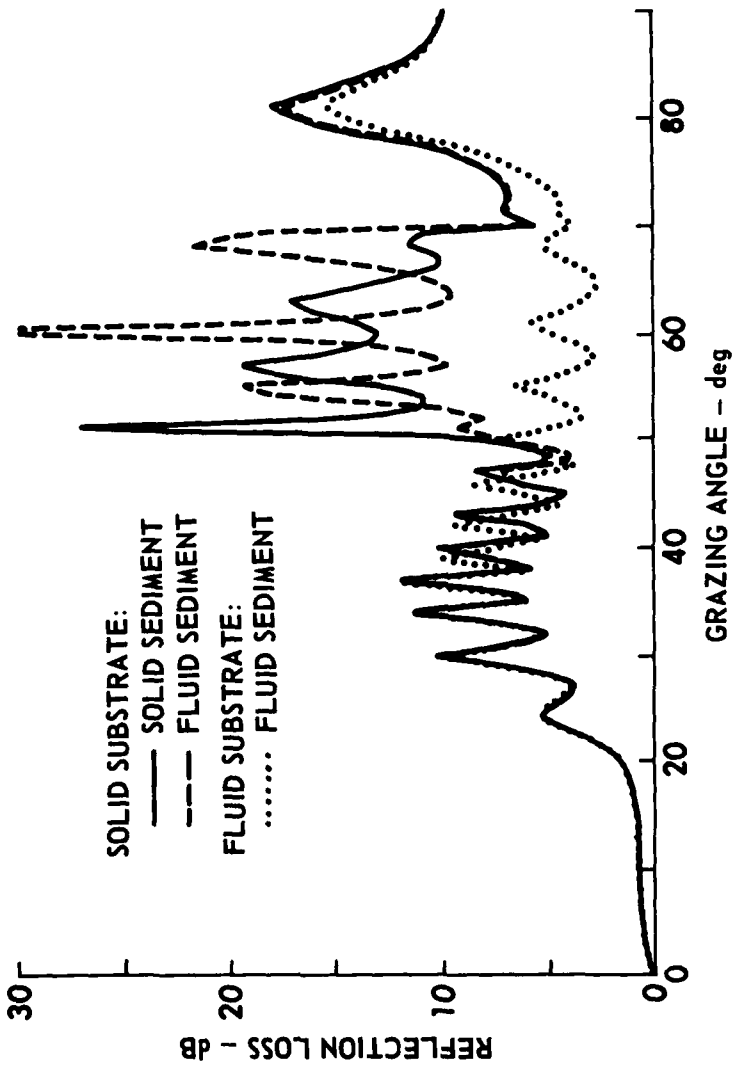

FIGURE 1
REFLECTION LOSS versus GRAZING ANGLE FOR A 518 m
THICK HYPOTHETICAL TURBIDITE LAYER AT 20 Hz

ARL:UT
AS-78-1735-S
PJV-GA
11-27-78

that sediment rigidity is negligible for this particular sediment structure at low grazing angles and at a frequency of 20 Hz.

Figure 2 shows RL for a thinner sediment layer, H = 252 m, at f = 20 Hz. The FS and SS cases are shown. Comparison of the solid (SS) and dashed (FS) curves shows that the presence of sediment rigidity produces the expected shift in the oscillatory structure between the critical angles, θ_s and θ_p. In addition, the SS case has an increased RL beginning at a minimum grazing angle, $\theta_o \approx 24°$, and extending up to about 45°. This increase in RL is entirely due to sediment rigidity. For grazing angles below θ_o the effect of sediment rigidity is negligible.

Figure 3 shows RL for the 252 m layer as a function of frequency at $\theta = 20° < \theta_o$. The frequency range is 10 to 100 Hz. A comparison of the SS and FS cases shows that for frequencies above 15 Hz sediment rigidity is negligible. Below 15 Hz the difference between the curves may not be meaningful since this is near the low frequency limit of the validity of the computational model.

A consideration of RL as a function of θ for sediment thicknesses less than 252 m reveals a relationship between H and θ_o. As H decreases, θ_o also decreases. Thus, as sediment thickness decreases, sediment rigidity affects RL at steadily lower grazing angles. In fact, sediment S wave excitation can be the dominant energy loss mechanism in thin sediment layers. This is illustrated in Fig. 4 which compares RL for the SS and FS cases at H = 36 m and f = 20 Hz. The angle θ_o is 0°. Sediment S wave excitation is responsible for the dramatic 20 dB increase in RL near $\theta = 12°$.

The dependence of RL on frequency for the same 36 m layer is shown in Fig. 5. The SS and FS cases are compared from 10 to 200 Hz at $\theta = 20°$. The SS case has high and low frequency regimes with strikingly different properties. At low frequencies the effects of sediment rigidity increase

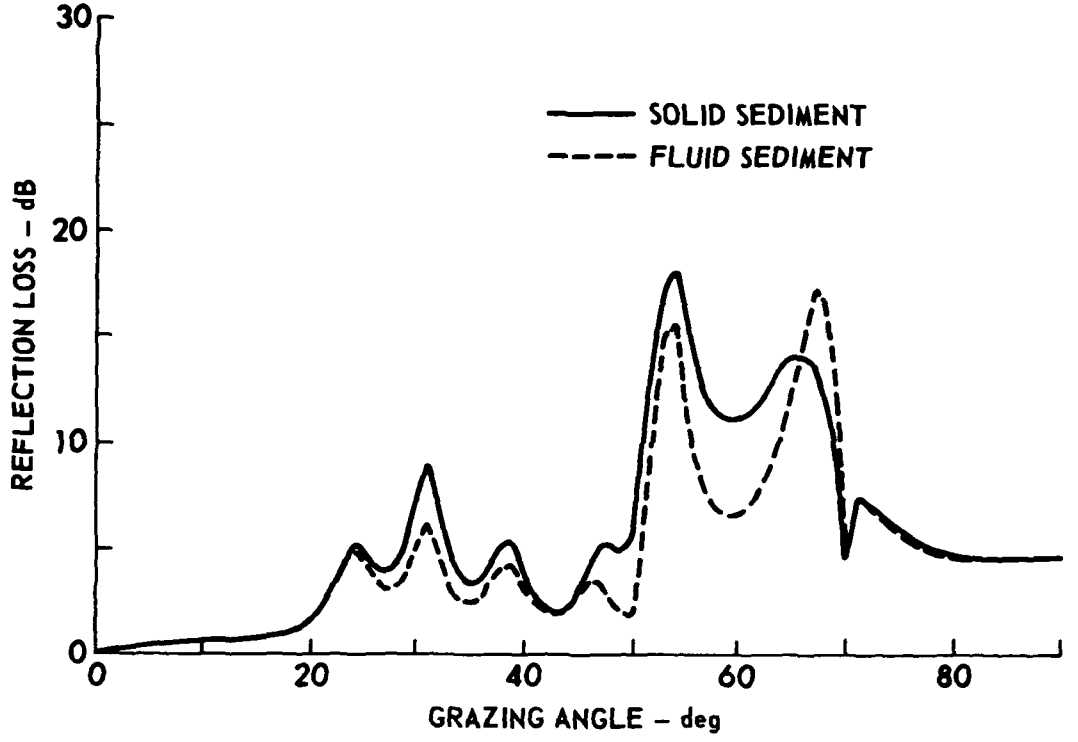

FIGURE 2
REFLECTION LOSS versus GRAZING ANGLE FOR A 252 m
THICK HYPOTHETICAL TURBIDITE LAYER AT 20 Hz

ARL:UT
AS-78-1737-S
PJV-GA
11-27-78

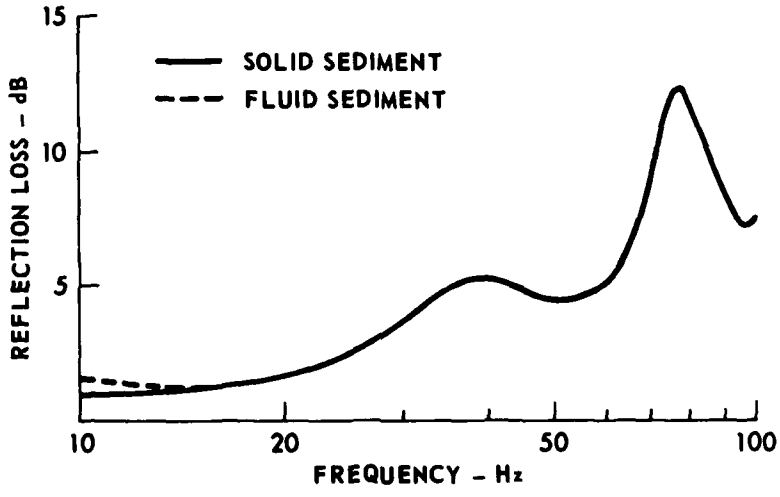

FIGURE 3
REFLECTION LOSS versus FREQUENCY FOR A 252 m
THICK HYPOTHETICAL TURBIDITE LAYER AT 20°

ARL:UT
AS-79-1815-P
PJV - GA
8 - 17 - 79

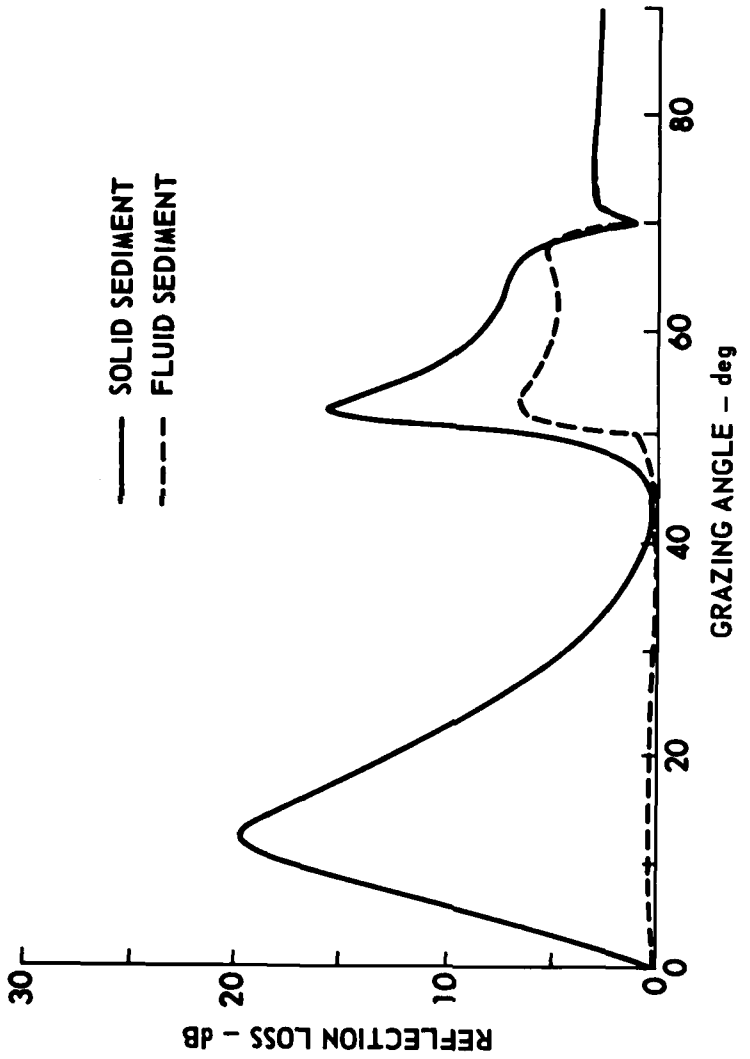

FIGURE 4
REFLECTION LOSS versus GRAZING ANGLE FOR A 36 m
THICK HYPOTHETICAL TURBIDITE LAYER AT 20 Hz

ARL:UT
AS-78-1738-S
PJV-GA
11-27-78

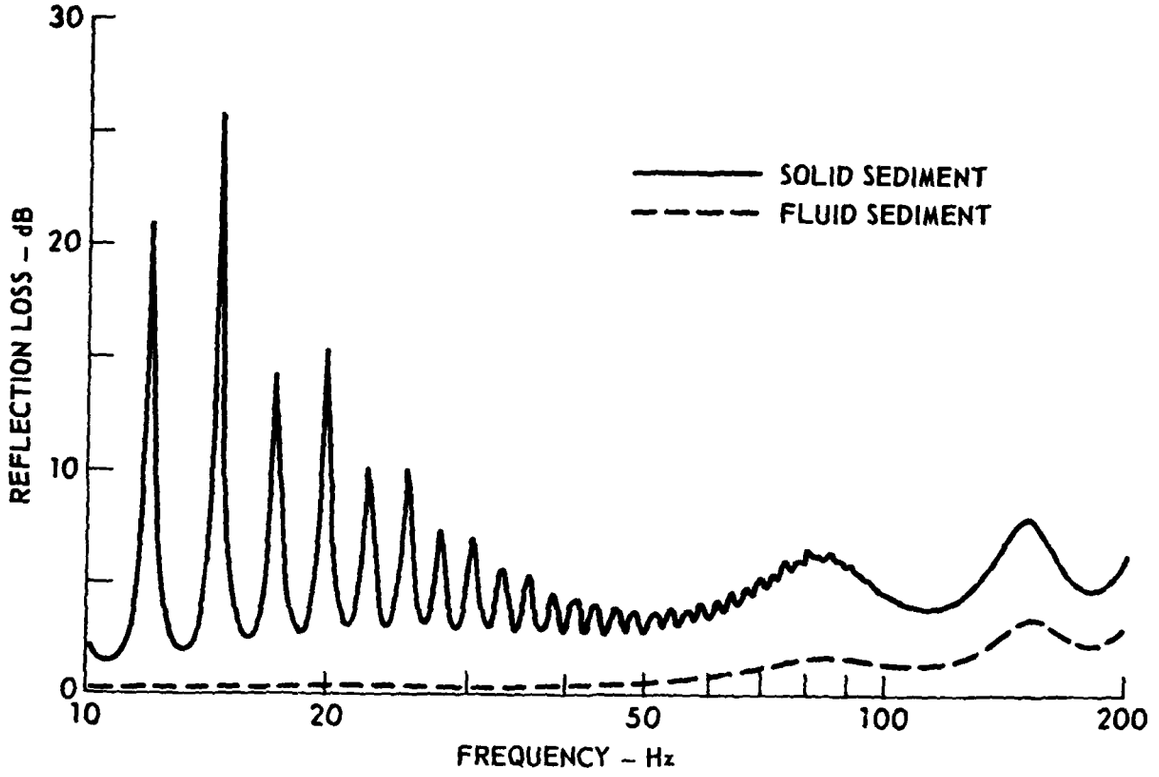

FIGURE 5
REFLECTION LOSS *versus* FREQUENCY FOR A 36 m
THICK HYPOTHETICAL TURBIDITE LAYER AT 20°

ARL-UT
AS-79-1123-S
PJV - GA
5 - 28 - 79

the level of RL, relative to the FS case, by about 3 dB, with additional very large peaks of up to 25 dB. The peaks repeat with an almost constant separation of 2.65 Hz. The magnitude of the peaks generally decreases with increasing frequency; however, any individual peak may be higher or lower than neighboring peaks. The peaks disappear by about 90 Hz and the high frequency regime, characterized by rather broad oscillations in RL, begins. The maxima of these broad oscillations are separated in frequency by about 65.5 Hz and occur in both the SS and FS cases. In this high frequency regime, sediment S wave excitation produces an almost constant increase in RL of about 4 dB.

The large peaks in the low frequency regime of Fig. 5 are associated with interference effects due to sediment S wave propagation. This identification is made by noting that the frequency interval between peaks is related to S wave parameters. One expects interference effects to recur when the relative phases of the waves involved change by 2π. The phase of the S wave, accumulated in traveling through the sediment and back, changes by 2π for a frequency change $\Delta f \simeq v_2/2H$, where v_2 is the average sediment S wave speed. (The sediment shear speed is so small that the S waves propagate nearly normal to the plane of stratification.) The measured separation between peaks is within 5% of the estimated value of Δf. The corresponding quantity for P waves (including the grazing angle correction) estimates a frequency change of 65.4 Hz, which is a factor of 30 too large to explain the peak separation. In addition, the decrease in peak height with frequency appears to be related to the increased attenuation of S waves with frequency. At 90 Hz the attenuation is estimated to be 23 dB for an S wave traveling one way through the sediment. This calculation predicts that S wave interference would be negligible above 90 Hz (maximum effect of 1%).

The gentle oscillations above 90 Hz in Fig. 5 are due to P wave interference effects. This conclusion is reached because the same oscillations are observed in both the SS and FS cases. The measured

separation between maxima is 65.5 Hz, which agrees very well with the estimated Δf = 65.4 Hz.

Figure 6 shows that sediment rigidity is still significant in the high frequency regime. The SS and FS cases are compared at H = 36 m and f = 200 Hz. The increase in RL due to sediment S wave excitation is significant (~4 dB) between 15° and 30°. The minimum grazing angle, θ_o, is about 5°.

Inspection of Fig. 5 near 20 Hz shows that the very large increase in RL seen in the SS case in Fig. 4 is due to the fortuitous location of one of the interference peaks at 20 Hz. For comparison with Fig. 4, RL is given at 21 Hz (minimum in RL) in Fig. 7. The increase in RL due to sediment S wave excitation is still present at low angles but its magnitude is 2 dB rather than 20 dB. This is still a significant increase in RL when compared to the RL≈0 for the fluid sediment case.

The dependence of θ_o on H gives an indication of the physical mechanism responsible for the increase in RL due to sediment rigidity. For a given grazing angle the compressional wave in the sediment has a turning point at a depth H_t. For a thick sediment layer H_t will be well above the sediment-substrate interface. As the grazing angle increases, H_t increases. At some critical angle θ_c, $H_t \simeq H$ and the compressional wave interacts with the sediment-substrate interface. As the thickness of the sediment layer decreases, the angle θ_c also decreases. This is the same qualitative behavior exhibited by the angle θ_o, above which sediment rigidity causes an increase in RL. This similarity suggests that sediment shear wave excitation by compressional wave conversion at the sediment-substrate interface produces the increase in RL.

Two other observations support this identification of P wave conversion at the sediment-substrate interface as the dominant mechanism for sediment S wave excitation. One concerns the negligible influence of the water-sediment interface while the other shows the importance of the substrate interface. S wave excitation at the water-sediment interface appears to be negligible. The properties of the water interface remained

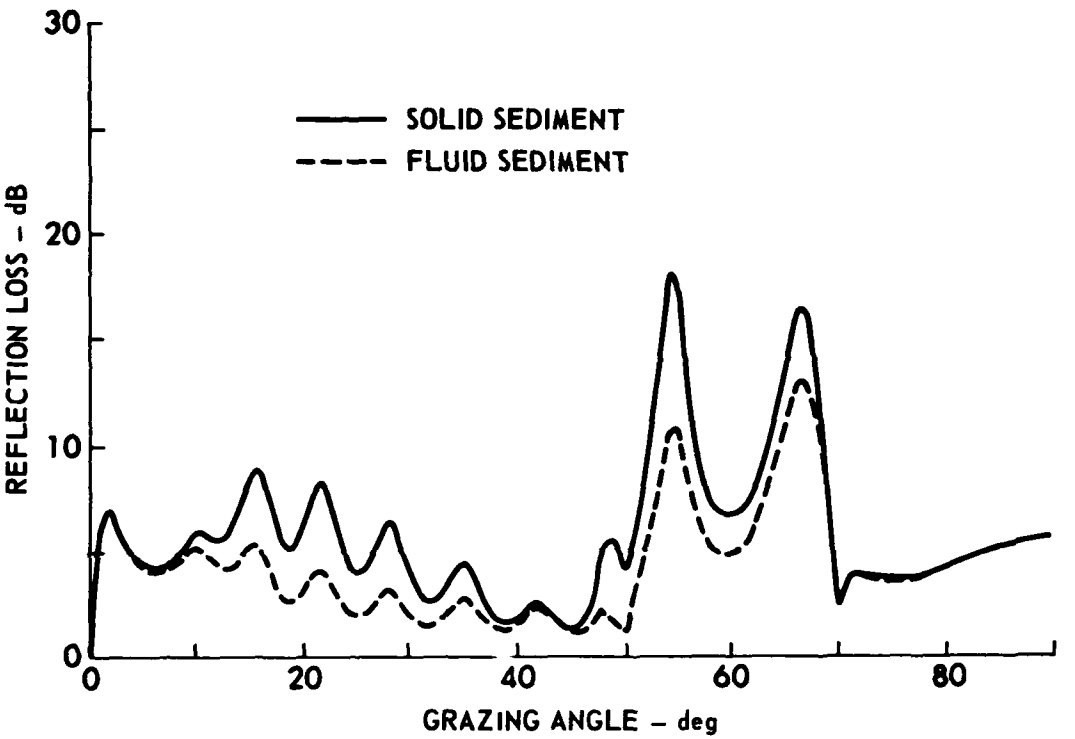

FIGURE 6
REFLECTION LOSS versus GRAZING ANGLE FOR A 36 m
THICK HYPOTHETICAL TURBIDITE LAYER AT 200 Hz

ARL:UT
AS-78-1739-S
PJV-GA
11-27-78

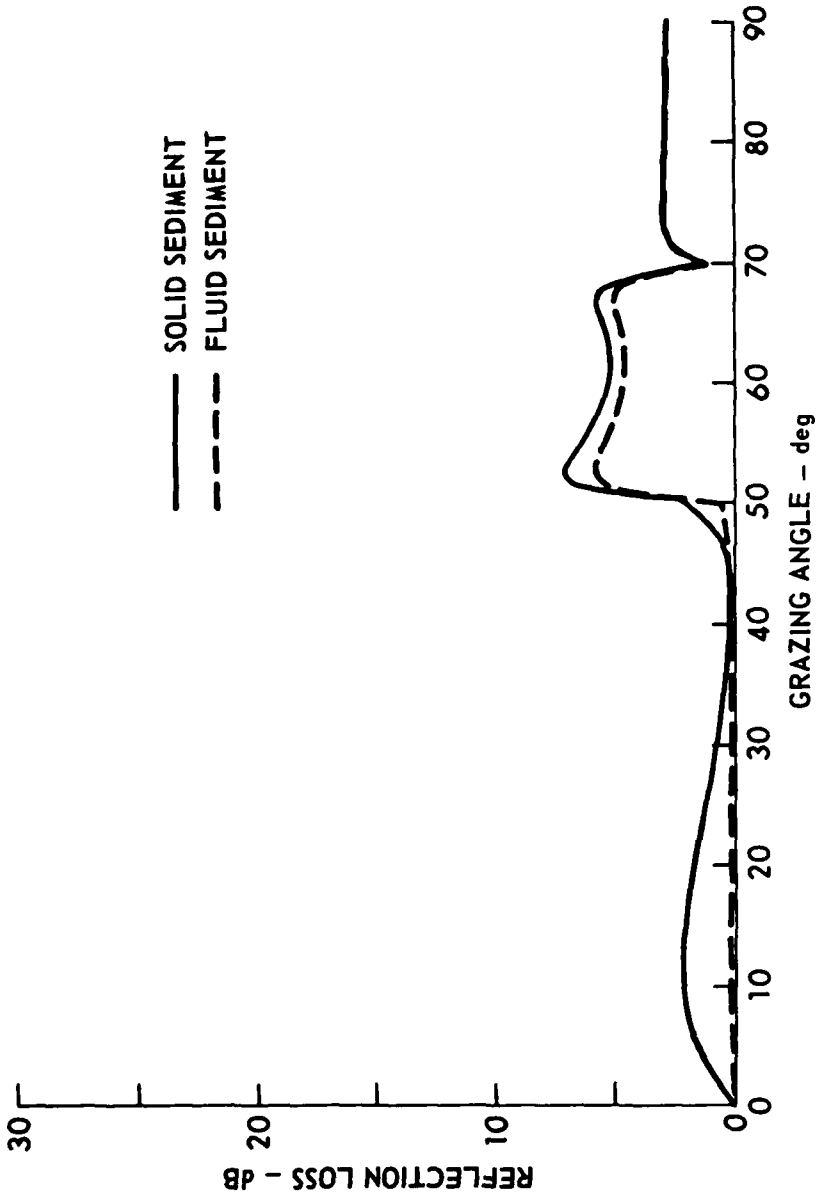

FIGURE 7
REFLECTION LOSS versus GRAZING ANGLE FOR A 36 m
THICK HYPOTHETICAL TURBIDITE LAYER AT 21 Hz

ARL:UT
AS-79-1122-S
PJV - GA
5 - 28 - 79

constant while the sediment thickness varied and large changes in RL due to sediment rigidity occurred. It is difficult to establish a causal relationship between something which remains constant and another quantity which changes significantly. The importance of the substrate interface is further indicated by the negligible difference between RL for the FF and SF cases and the large changes seen between the SS and FS cases. This indicates that the nature of the substrate is important. Since the substrate enters only through the sediment-substrate interface conditions, this indicates that sediment S waves originate at the substrate interface.

The results of this section lead to an empirical classification of sediments into thick and thin layers based on the effect of sediment rigidity. The behavior of thin layers can be further split into high frequency and low frequency regimes, based on S wave attenuation. For thick sediments little energy is transferred to sediment S waves and the sediment can accurately be treated as a fluid at low grazing angles. For a thin sediment significant energy can appear in sediment S waves. Sediment rigidity is not negligible and the sediment must be treated as a solid. For thin sediments at low frequencies (S wave attenuation less than 20 dB across the layer) interference effects due to S wave propagation are important. Large (>20 dB) increases in RL are possible at particular frequencies. At high frequencies (S wave attenuation larger than 20 dB across the layer) sediment S wave propagation can be neglected. Significant energy can still be lost to S waves that are totally absorbed within the sediment.

III. MECHANISM OF SEDIMENT SHEAR WAVE EXCITATION

In this section a qualitative ray model of P and S wave propagation in a solid sediment layer is developed. The qualitative predictions of this model are tested using the wave theory computational model. The classification scheme of the previous section is predicted by the ray model and is made more understandable. Basic to the construction of the ray model is an understanding of the effect of sediment rigidity on the reflection and transmission coefficients at the water-sediment and sediment-substrate interfaces. These coefficients are examined using a small parameter expansion based on the relatively small S wave speeds in marine sediments. This expansion theory leads to a detailed understanding of the excitation mechanism of sediment S waves.

A. Expansion Theory of Reflection and Transmission Coefficients

The following conventions and definitions are used. Subscripts 1, 2, and 3 identify quantities in the water, sediment, and substrate, respectively. For simplicity we assume a horizontally stratified ocean bottom with homogeneous media. A harmonic time dependence with angular frequency ω is assumed. Compressional wave speeds are c_j, S wave speeds are v_j, and densities are ρ_j. Wave numbers are defined as: $K_j=\omega/c_j$, $B_j=\omega/v_j$, $k=K\cos\theta$, $\kappa_j=[K_j^2-k^2]^{1/2}$, and $\beta_j=[B_j^2-k^2]^{1/2}$, where θ is the grazing angle of the incident ray in the water. Subscripts p and s will identify reflection and transmission coefficients for P and S waves, respectively. The water-sediment interface will be indicated by W/S and the sediment-substrate interface by S/S.

The z axis increases downward from the water into the sediment. The displacement $\underline{u}_j$ is defined in terms of a scalar potential, $\phi_j=\phi_j(z)e^{i(kx-\omega t)}$, and a vector potential, $\underline{\Psi}_j=\hat{y}X_j(z)e^{i(kx-\omega t)}$, by $\underline{u}_j=\underline{\nabla}\Phi_j+\underline{\nabla}\times\underline{\Psi}_j$, where

$\hat{y}$ is a unit vector along the y axis. The depth dependencies are given by $\phi_j = W_j^- e^{i\kappa_j z} + W_j^+ e^{-i\kappa_j z}$, and $X_j = V_j^- e^{i\beta_j z} + V_j^+ e^{-i\beta_j z}$, where W_j^- and V_j^- are the amplitudes of the downward propagating waves and W_j^+ and V_j^+ are the amplitudes of the upgoing plane waves.

The basis of our study of the reflection and transmission coefficients is an expansion in the small parameter $\epsilon = v_2/c_1$. Only the lowest order correction terms in ϵ will be kept. This will be an excellent approximation at the W/S interface where the surficial shear wave velocities are between 50 m/sec and 150 m/sec, giving $0.03 < \epsilon < 0.10$. The expansion parameter is not as good at the S/S interface because of the larger S wave velocity due to positive shear speed gradients.[10] Higher order corrections would then be needed for accurate values of the reflection and transmission coefficients at the S/S interface. However, the lowest order corrections contain the qualitative results we are seeking and are adequate for thin layers. For the turbidite layer of the previous section ϵ varies from 0.076 at the W/S interface to 0.185 at 36 m, 0.256 at 120 m, and 0.406 at 518 m. Even at 518 m the second order terms contribute only 15% corrections compared to the 40% corrections due to first order terms.

Beginning at the W/S interface with a unity amplitude sound wave incident from the water, $\phi_1 = (e^{i\kappa_1 z} + R_{p12} e^{-i\kappa_1 z}) e^{i(kx-\omega t)}$, we obtain

$$R_{p12} = R_{12}^{(o)} - 2\epsilon^2 T_{12}^{(o)} T_{21}^{(o)} \cos^2\theta \quad , \tag{1}$$

$$T_{p12} = T_{12}^{(o)} + 2\epsilon^2 T_{12}^{(o)} R_{21}^{(o)} \cos^2\theta \quad , \tag{2}$$

$$T_{s12} = 2\epsilon^2 T_{12}^{(o)} (\kappa_2/k) \cos^2\theta \quad , \tag{3}$$

where $R_{ij}^{(o)} = (\kappa_i \rho_j - \kappa_j \rho_i)/(\kappa_i \rho_j + \kappa_j \rho_i)$ and $T_{ij}^{(o)} = 2\kappa_i \rho_i/(\kappa_i \rho_j + \kappa_j \rho_i)$ are the zero order reflection and transmission coefficients obtained for a fluid sediment with the P wave incident from medium i.[16]

Equations (1) through (3) show that, as far as the incident sound wave is concerned, the sediment can be accurately treated as a fluid. Equations (1) and (2) show that sediment rigidity produces only second order (ε^2) corrections to the fluid-fluid interface reflection and transmission coefficients. Equation (3) shows that the excited sediment shear wave amplitude is of order ε^2 and thus contains little incident energy.

The downward propagating P and S waves next strike the S/S interface. For the incident P wave we find

$$R_{p23} = R^{(o)}_{p23} - \varepsilon\Gamma_p \eta \cos\theta \quad , \tag{4}$$

$$T^{(o)}_{p23} = T^{(o)}_{p23} - \varepsilon\Gamma_p \tau_p \cos\theta \quad , \tag{5}$$

$$R_{s23} = -2\varepsilon\Gamma_p \cos\theta \quad , \tag{6}$$

$$T_{s23} = T^{(o)}_{s23} - \varepsilon\Gamma_p \tau_s \cos\theta \quad . \tag{7}$$

For an incident S wave we have

$$r_{p23} = \eta(1-\varepsilon\Gamma_s\cos\theta) \quad , \tag{8}$$

$$t_{p23} = \tau_p(1-\varepsilon\Gamma_s\cos\theta) \quad , \tag{9}$$

$$r_{s23} = 1 - 2\varepsilon\Gamma_s\cos\theta \quad , \tag{10}$$

$$t_{s23} = \tau_s(1-\varepsilon\Gamma_s\cos\theta) \quad . \tag{11}$$

In Eqs. 4 through (11) we have used the quantities

$$\Gamma_s = \left(R^{(o)}_{p23} - T^{(o)}_{p23} + \beta_3 T^{(o)}_{s23} \Big/ k\right) \Big/ 2 \quad , \tag{12}$$

$$\Gamma_p = \Gamma_s + 1/2 \quad , \tag{13}$$

$$\eta = 2k\Gamma_p/\kappa_2 \quad , \tag{14}$$

$$\tau_p = \frac{-k}{\kappa_1}\left[\left(1-R^{(o)}_{p23}\right)\rho_2\kappa_2\Big/\rho_3\kappa_3 - T^{(o)}_{p23} + T^{(o)}_{s23}\kappa_2\beta_3\Big/\kappa_3 k\right] \quad , \tag{15}$$

$$\tau_s = \left(1-R^{(o)}_{p23}\right)\rho_2/\rho_3 + T^{(o)}_{s23}k/\kappa_2 + T^{(o)}_{p23} \quad , \tag{16}$$

and the zero order reflection and transmission coefficients for a P wave, with horizontal wave number k, incident from a fluid sediment[16,17]

$$R^{(o)}_{p23} = \left|\rho_3\kappa_2\left[\left(1-2a^2\right)^2 + 4a^4\kappa_2\beta_3\Big/k^2\right] - \rho_2\kappa_3\right|\Big/D \quad , \tag{17}$$

$$T^{(o)}_{p23} = 2\rho_2\kappa_2(1-2a^2)\Big/D \quad , \tag{18}$$

$$T^{(o)}_{s23} = 4\rho_2\kappa_2 a^2\kappa_3\Big/kD \quad , \tag{19}$$

where $a=v_3\cos\theta/c_o$, and

$$D = \rho_3\kappa_2\left[\left(1-2a^2\right)^2 + 4a^4\kappa_2\beta_3\Big/k^2\right] + \rho_2\kappa_3 \quad . \tag{20}$$

Equations (4) through (11) show that sediment rigidity can be important at the S/S interface. According to Eq. (6) the P wave incident upon the S/S interface excites a first order (ε^1) S wave in the sediment. Equations (4), (5), and (7) show that the reflected P wave and P and S waves transmitted into the substrate also have first order corrections to their amplitudes. Recalling that the S wave excited at the W/S interface is of order ε^2 [Eq. (3)], Eqs. (8) through (10) show that the reflected and transmitted waves due to it are at most of order ε^2. These are then a correction to the larger, order ε^1, corrections due to P wave conversion at the S/S interface. The presence of gradients will increase the relative effectiveness of the S/S interface.

Equations (8) through (11) show an apparent inconsistency. The incident S wave is perfectly reflected to order ε^0 and yet sets up other reflected and transmitted waves whose amplitudes are also of order ε^0. The inconsistency disappears when the total energy flux at the S/S interface is considered. Recalling that the energy flux is proportional to the inverse of the wave speed, the incident and reflected S waves in the sediment have their energy flux proportional to ε^{-1}, while the flux of the other wave is, to lowest order, proportional to ε^0. The S waves, then, carry one order higher energy flux than the other waves even though all the amplitudes are the same order. To order ε^{-1}, the incident and reflected S waves conserve energy flux. To the next order, ε^0, the part of the S wave energy that is not perfectly reflected (ε^1 corrections to the amplitude) provides some order ε^0 energy which appears in the lowest order energy flux of the other waves.

We next consider incident S and P waves in the sediment striking the W/S interface. The computed reflection and transmission coefficients are

$$R_{p21} = R_{21}^{(o)} + 2\varepsilon^2 T_{12} T_{21} \cos^2\theta \quad , \tag{21}$$

$$T_{p21} = T_{21}^{(o)} + 2\varepsilon^2 T_{21} R_{12} \cos^2\theta \quad , \tag{22}$$

$$R_{s21} = 2\varepsilon^2 T_{21}^{(o)} K_1 \cos^2\theta \Big/ k \quad , \tag{23}$$

for an incident P wave and

$$r_{p21} = -2\varepsilon\left(1-R_{21}^{(o)}\right)\cos\theta \quad , \tag{24}$$

$$t_{p21} = 2\varepsilon T_{21}^{(o)} \cos\theta \quad , \tag{25}$$

$$r_{s21} = -1 \quad , \tag{26}$$

for an incident S wave. The lowest order corrections to Eq. (26) are of order ε^3.

Equations (21) through (23) give the same qualitative results as Eqs. (1) through (3). Both sets of equations show that the corrections due to sediment rigidity are of order ε^2 at the W/S interface when a P wave is incident, i.e., the sediment can be accurately treated as a fluid at the W/S interface whenever a P wave is incident. Recalling that the incident S wave is at most of order ε [Eqs. (3), (6), (10)], the corrections to P wave amplitudes due to S wave conversion are at most of order ε^2 [Eqs. (24) and (25)]. This leads to the conclusion that the sediment properties at the W/S interface are very simple. It is a fluid as far as P waves are concerned. The S wave incident from below is perfectly reflected with a 180° phase shift [Eq. (26)].

The mechanism for sediment S wave excitation to lowest order in ε can now be deduced from the combined action of the reflection and transmission coefficients. As far as p waves are concerned, the sediment is a fluid at the W/S interface and negligible energy is transferred into S waves. An order ε S wave is excited in the sediment by the P wave striking the S/S interface. The sediment S wave has no further effect. It is essentially perfectly reflected from the W/S and S/S interfaces and produces, at most, order ε^2 corrections to the P wave returned to the water column. The P wave reflected from the S/S interface does, however, have an important role to play. It picks up an order ε correction to its amplitude at the S/S interface. This correction travels through the W/S interface and affects the energy returned to the water.

The following picture now emerges. Sediment rigidity affects bottom reflection loss by means of energy transferred to sediment shear waves at the sediment-substrate interface. Sediment compressional waves play a major role, in that they excite the shear wave at the sediment-substrate interface and are responsible for carrying the influence of the shear wave back through the sediment and into the water. The major effect of sediment rigidity is then to provide an energy sink at the sediment-substrate interface. We note that this situation will be slightly modified if higher order (ε^2 and above) corrections are important.

The empirical classification of sediments as thick or thin can now be understood and quantified. For a thick sediment layer the P wave has its turning point well above the S/S interface, and it does not significantly interact with the S/S interface. Since only order ε^2 corrections are possible due to the refracted P waves at the W/S interface, sediment rigidity has a negligible effect on RL. In this case the sediment can be accurately treated as a fluid. For a thin sediment layer, the P wave interacts significantly with the S/S interface, where sediment S waves are excited. In this case the sediment must be treated as a solid. The question of whether a sediment layer is thick or thin is then translated into the more easily quantified question of whether the P wave interacts with the sediment-substrate interface (thick), or not (thin).

The reason for the similarity of the FF and SF cases, noted in the previous section, can now be understood. Equations (21) through (23) can also be applied to the S/S interface when the substrate is taken to be a fluid; only order ε^2 corrections are possible. Negligible energy is transferred to sediment S waves. The sediment can be accurately treated as fluid whenever the substrate is a fluid--this leads to the conclusion that a solid substrate is required for sediment rigidity to affect RL. This statement can be generalized to include the possibility of S wave excitation at an interface within a layered sediment, provided the layer has a significantly larger shear velocity.

B. Qualitative Ray Picture

The transmission and reflection coefficients derived above will now be applied to the development of a ray model of the qualitative effects of sediment rigidity. The reflection and transmission coefficients obtained above will be used to determine the ray amplitudes at each interface. A single homogeneous sediment layer will be considered. The expansion parameter will be subscripted by U or L to identify the values at the W/S or S/S interfaces, respectively. This allows the corrections,

due to sediment rigidity, to be identified at each interface and allows us to consider the qualitative effects of gradients in shear speed by setting $\varepsilon_L > \varepsilon_u$.

The results are shown schematically in Figs. 8, 9, and 10. The solid lines are the ray paths of P waves and the dashed lines are the ray paths of S waves. Since the S wave speed in marine sediments is so small compared to the sound speed in water, the S wave rays are almost normal to the plane of stratification. Figure 8 shows the effect of sediment rigidity if S wave attenuation is high enough for the S wave to be totally absorbed before crossing the layer. Figure 9 shows the additional ray paths resulting from the first reflection of the sediment S waves and Figure 10 shows those due to the second reflection.

In Figure 8 the S wave attenuation is high enough for an S wave to be completely absorbed in traveling one way through the sediment. The incoming water wave is reflected at the W/S interface with corrections of order ε_u^2 [Eq. (1)]. The transmitted P wave also has an order ε_u^2 correction [Eq. (2)] which is neglected. A small amplitude S wave of order ε_u^2 is also excited [Eq. (3)]. The transmitted P wave strikes the S/S interface where an order $\varepsilon_L+\varepsilon_L^2$ S wave is excited [Eq. (6)]. The reflected P wave and the substrate P and S waves suffer order $\varepsilon_L+\varepsilon_L^2$ corrections [Eqs. (4), (5), and (7)]. The P wave carries its corrected amplitude back through the sediment to the W/S interface. Here a small, order ε_u^2 S wave is excited [Eq. (23)]. The transmitted P wave carries the $\varepsilon_L+\varepsilon_L^2$ corrections into the water and also picks up a negligible order ε_u^2 correction from the W/S interface. The reflected P wave carries corrections of the order $\varepsilon_L+\varepsilon_L^2$ back down through the sediment where it interacts with the S/S interface and the process repeats. The directly reflected ray and the rays excited in the water by the sediment P waves combine to form a wave, A_o, which is of order ε^o with $\varepsilon_L+\varepsilon_L^2$ corrections.

Figure 9 shows the additional rays set up when the S wave attenuation is reduced to allow the sediment S waves to strike one interface before being absorbed. The order ε_u^2 ray originating at the W/S interface is

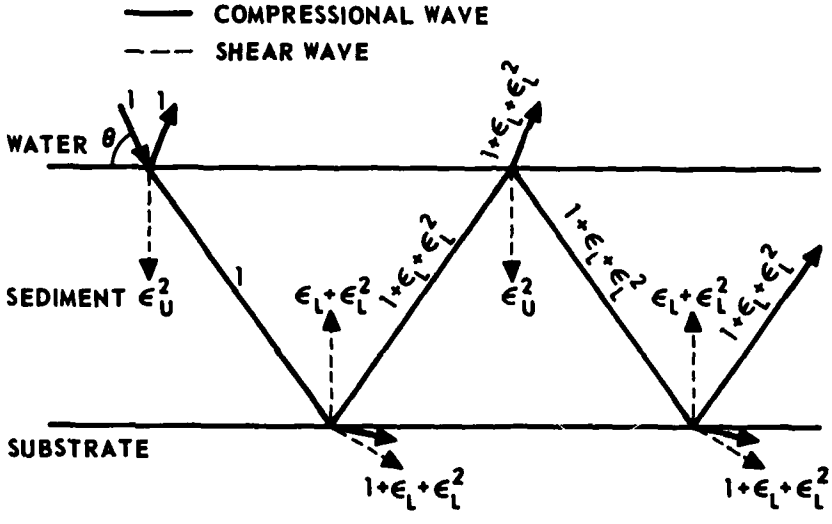

FIGURE 8
THE RAY PICTURE: SEDIMENT SHEAR WAVE
ABSORBED BEFORE REFLECTION

ARL:UT
AS-79-1816-P
PJV-GA
8-17-79

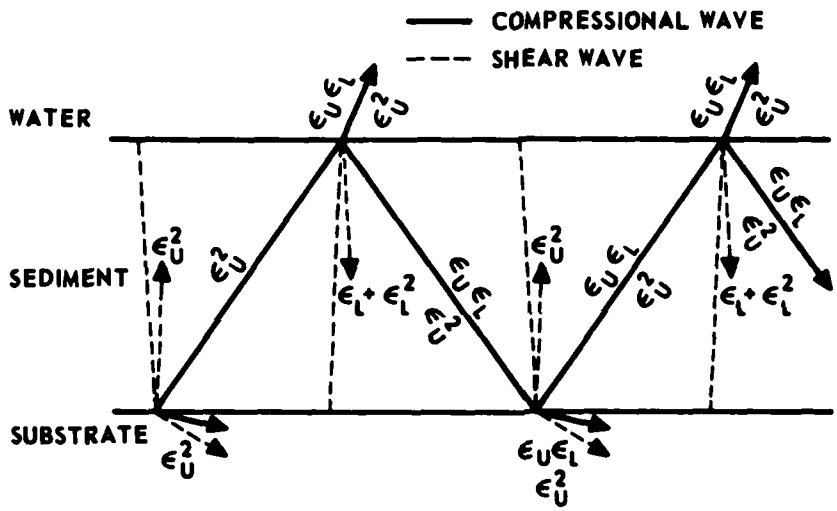

FIGURE 9
THE RAY PICTURE: THE FIRST REFLECTION
OF THE SEDIMENT SHEAR WAVES

ARL:UT
AS-79-1817-P
PJV-GA
8-17-79

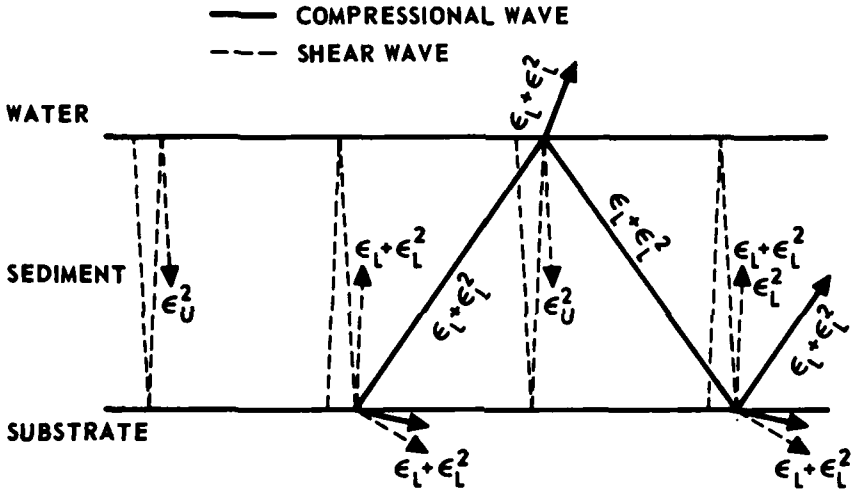

FIGURE 10
THE RAY PICTURE: THE SECOND REFLECTION
OF THE SEDIMENT SHEAR WAVES

ARL:UT
AS-79-1818-P
PJV - GA
8 - 17 - 79

totally reflected from the substrate [Eq. (8)] and carries its ϵ_u^2 magnitude. Corrections of order $\epsilon_u^2\epsilon_L$ are neglected. It sets up order ϵ_u^2 P and S waves in the substrate and a reflected P wave of order ϵ_u^2 in the sediment. The P wave transmits its ϵ_u^2 magnitude into the water and into a reflected P wave at the W/S interface [Eqs. (21) and (22)]. The reflected S wave is of order ϵ_u^2 and is neglected [Eq. (23)]. The downward propagating P wave strikes the S/S interface where it sets up order ϵ_u^2 waves in the substrate and an order ϵ_u^2 reflected P wave [Eqs. (4), (5), and (7)]. No significant S wave is excited in the sediment [Eq. (6)]. The upgoing P wave then continues the process. The S wave originating at the substrate interface is totally reflected from the W/S interface [Eq. (26)] and retains its order $\epsilon_L+\epsilon_L^2$ magnitude. A reflected P wave of order $\epsilon_u\epsilon_L$ is excited [Eq. (24)] along with a transmitted P wave of amplitude $\epsilon_u\epsilon_L$ in the water [Eq. (25)]. The reflected P wave carries its magnitude through a reflection at the S/S interface [Eq. (4)] where it also excites P and S waves of order $\epsilon_u\epsilon_L$ in the substrate [Eqs. (5) and (7)]. No significant sediment S wave is set up [Eq. (6)]. The upward traveling P wave is again reflected from the W/S interface. The reflected sediment P wave and the transmitted wave in the water carry an order $\epsilon_u\epsilon_L$ magnitude [Eqs. (21) and (22)]. No significant S wave is excited [Eq. (23)]. The P wave then continues the process. The sum of the rays returned to the water sets up a wave A_2, whose magnitude is second order, i.e., order ϵ_u^2 or $\epsilon_u\epsilon_L$.

Figure 10 shows the situation for an attenuation small enough to allow the sediment S waves to be reflected a second time before being absorbed. The S wave originating at the W/S interface produces negligible effects when it strikes the W/S interface. The reflected S wave retains its order ϵ_u^2 magnitude and no significant P waves are excited [Eqs. (24), (25), and (26)]. The S wave originating at the S/S interface does produce additional corrections to the energy returned to the water. On striking the S/S interface it is reflected with its order $\epsilon_L+\epsilon_L^2$ magnitude [Eq. (10)]. It excites P and S waves in the substrate and a reflected P wave in the sediment, all of order $\epsilon_L+\epsilon_L^2$ [Eqs. (8), (9), and (11)]. The P wave in the sediment travels through the sediment to the water

interface where it is reflected, retaining its order $\epsilon_L+\epsilon_L^2$ [Eqs. (21) and (22)]; it does not excite a significant S wave [Eq. (23)]. The downward propagating P wave is reflected from the substrate interface, retaining its $\epsilon_L+\epsilon_L^2$ magnitude, and sets up order $\epsilon_L+\epsilon_L^2$ waves in the substrate [Eqs. (4), (5), and (7)]. The reflected P wave then continues the process and an S wave of order ϵ_L^2 is also excited in the sediment [Eq. (6)]. This S wave produces no further effects since it is absorbed before reaching the W/S interface. This can be seen by recalling that the magnitude of this S wave is proportional to the P wave which struck the S/S interface. The magnitude of the P wave is in turn proportional to the magnitude of the S wave which originated at the S/S interface and has traveled up and back through the sediment. The maximum amplitude of the newly excited S wave then corresponds to the amplitude of the twice reflected shear wave. By hypothesis (in this example) an S wave is absorbed before its third reflection. Hence, the new S wave will be absorbed before it reaches the W/S interface. The rays returning to the water in Fig. 10 combine to form a wave A_1, whose magnitude is of order $\epsilon_L+\epsilon_L^2$. This wave contributes the largest correction to the A_o wave of Fig. 8.

The qualitative ray model developed in Figs. 8 through 10 can be used to understand many of the features of Fig. 5, which shows the dependence of RL on frequency for the 36 m turbidite layer. Figure 8 applies to the high frequency regime where shear wave attenuation is large. Figures 9 and 10 apply at lower frequencies and explain the origin of the oscillatory structure. A generalization of Figs. 8 through 10 to very low frequencies shows the possibility of very large interference effects.

According to Fig. 8 the high frequency behavior of R is due to energy returning to the water in the A_o wave which carries the effects of S wave excitation at the S/S interface through corrections of order ϵ_L and ϵ_L^2. The magnitude of the A_o wave depends on the phase difference between its constituent directly reflected component and the component due to the propagation of the P wave through the sediment. The magnitude

of R is the result of interference between these two components of A_o. This is the source of the broad oscillations at high frequencies seen in both the fluid sediment and solid sediment curves of Fig. 5. The almost constant offset of 4 dB between the two curves is due to the order $\varepsilon_L+\varepsilon_L^2$ correction to the magnitude of the wave transmitted into the water by the P wave in the sediment. The S wave excited at the W/S interface has a negligible effect on RL.

Two additional interfering waves occur in the water when the frequency is reduced to allow the S waves to reflect once from an interface. These are the $\varepsilon_u\varepsilon_L$ and ε_u^2 contributions to A_2 in Fig. 9. These contributions are small compared to the ε_L corrections due to A_o. The S wave excited at the W/S interface results in a series of rays returning to the water with magnitude of order ε_u^2. The coherent sum of these waves has a phase which depends on both P and S wave propagation. The S wave dependence occurs through a phase $\phi_1=\omega H/v_2$ due to traveling one way through the sediment. The phase due to the P wave varies more slowly with frequency. The S wave excited at the S/S interface results in a series of rays whose sum is of order $\varepsilon_u\varepsilon_L$ and whose phase also has the usual P wave part and the S wave part, $\phi_1=\omega H/v_2$. The S wave parts of the phase introduce a phase shift of 2π in a frequency change $\Delta f_1=v_2/H$. This results in a rapid oscillation in RL as frequency changes, compared to the P wave oscillations. An oscillation with this frequency change can be observed near 90 Hz in Fig. 5. The modulation of the peak heights at lower frequencies also has this recurrence frequency.

The additional set of rays introduced back into the water by the second S wave reflection, the A_1 wave in Fig. 10, are more important. They have a magnitude of $\varepsilon_L+\varepsilon_L^2$ and are thus larger than those produced by the first S wave reflection. They have the usual P wave phase change and also an S wave related phase of $\phi_2=2\omega H/v_2$ due to traveling through the sediment and back. This S wave phase results in a very rapid oscillation in RL as the frequency is changed. The frequency separation between maxima is $\Delta f_2=v_2/2H$, which is half of Δf_1. The magnitude of A_1

is larger than that of A_2 so that it dominates the interference structure of RL as a function of frequency. Thus, the oscillation at Δf_2 is stronger in Fig. 5 than that at Δf_1.

The behavior of RL at lower frequencies where S wave attenuation is very small can be deduced from a generalization of Figs. 8 through 10. The S waves reflect many times in the sediment. Additional waves of each type ($\varepsilon_L+\varepsilon_L^2$, $\varepsilon_u\varepsilon_L$, ε_u^2) are produced by the interactions at the W/S and S/S interfaces. Within each type (ε_u^2 for example) the successive waves have a relative phase shift of $\Delta\phi_2$ due to the additional propagation distance of the S wave. This allows a powerful interference phenomenon to develop. The A_1 wave will interfere destructively with the A_o wave at some frequency and at frequencies separated by integer multiples of Δf_2. (Small phase shifts due to effects other than S wave propagation are assumed to be more slowly varying with frequency.) At low frequencies the magnitude of the sum of all the in-phase A_1 waves can result in an order ε^o resultant amplitude and hence a very large cancellation of the A_o wave. This is the source of the very large RL peaks in Fig. 5.

For a homogeneous layer ($\varepsilon_u=\varepsilon_L=\varepsilon$) Figs. 8 through 10 show that only three kinds of waves emerge from the water-sediment interface. Figure 8 shows the largest of these. The directly reflected ray and the series of rays carrying a magnitude of order $1+\varepsilon+\varepsilon^2$ combine to form a single wave, the A_o wave. By itself the A_o wave contains the basic P wave interference structure and is responsible for the gentle oscillation structure at high frequencies in Fig. 5. The A_o wave also contains a correction to its magnitude of order $\varepsilon+\varepsilon^2$ due to the S wave excited at the substrate interface by the P wave. The phase of the A_o wave does not, however, contain a part due to S wave propagation. Thus the A_o wave contains an increase in RL due to sediment rigidity, but carries the basic phase of the P wave. The second kind of wave, the A_1 wave, is formed by the series of rays of order $\varepsilon+\varepsilon^2$ shown in Fig. 10. It is the most important correction to the A_o wave. Its magnitude is linear in ε

to lowest order while its phase contains the two-way S wave phase ϕ_2. The interference between the A_o and A_1 waves produces the rapid oscillations in RL as a function of frequency seen in Fig. 5. The third kind of wave, the A_2 wave, is formed by the series of rays of order ϵ^2 in Fig. 9. Since its magnitude is of order ϵ^2 it produces only small corrections compared to those due to the A_1 wave. The phase of the A_2 wave contains the one-way S wave phase, ϕ_1. The interference of this wave with the A_o and A_2 waves produces the modulation on the rapid oscillations in Fig. 5.

The ray model also predicts that the A_1 wave contributions should die out more rapidly than the A_2 contributions as frequency increases. Figures 9 and 10 show that the magnitude of these contributions depends on the attenuation suffered by the S wave in traveling through the sediment. The A_1 wave (Fig. 10) depends on the two-way total attenuation while the A_2 wave (Fig. 9) depends only on the one-way total attenuation. As S wave attenuation increases with frequency, the A_1 wave will decrease in magnitude more rapidly than the A_2 wave.

Finally, the ray picture shows the importance of S wave excitation by P wave conversion at the substrate interface. All corrections of order ϵ occur because of the initial interaction of the P wave with the substrate in Fig. 8. The order ϵ corrections in the A_o wave are clearly due to this interaction (Fig. 8). The A_1 wave is excited by S waves set up by the initial P wave interaction (Fig. 10). Part of the A_2 wave, the $\epsilon_u\epsilon_L$ contribution in Fig. 9, is also due to this initial P wave. These contributions to the reflected wave would all decrease in magnitude if the P wave amplitude were to be diminished. The remaining part of A_2, that labeled ϵ_u^2 in Fig. 9, while basically set up by P wave conversion at the water interface, also depends on the P wave traveling through the sediment layer. The same P wave conditions which would make the $\epsilon_u\epsilon_L$ wave unimportant would also affect this contribution to A_2 in the same manner. Thus, it is crucial for the P wave amplitude at the sediment-substrate interface to be significant if sediment rigidity is going to have an important effect on RL.

C. Verification of Ray Model

In this section the computational model will be used to test some of the qualitative predictions of the ray model. The dependence of R on frequency produced by the computational model will be used to extract the magnitudes of the A_o, A_1, and A_2 waves. This is accomplished by using the interference structure to separate the three waves. Homogeneous layers will be treated at frequencies near 15 Hz and a grazing angle of 20°. Tables II and III, profiles 1 through 4, give the parameters of the layers studied. The water parameters were $\rho_1 = 1.053$ g/cm^3, $c_1 = 1540$ m/sec. Parameter ranges are chosen to illustrate the features of the ray model and do not particularly represent parameter ranges in marine sediments.

The reflection coefficient is assumed to be of the form

$$|R| = A_o + A_1 \cos\phi_2 + A_2 \cos(\phi_1+\mu) \quad , \tag{27}$$

where A_o, A_1, and A_2 are the amplitudes of the A_o (order $1+\varepsilon$), A_1 (order ε) and A_2 (order ε^2) waves, and μ is a frequency independent phase difference between the A_1 and A_2 waves. This form for $|R|$ assumes that $\phi_1=\omega H/v_2$ and $\phi_2=\omega 2H/v_2$ contain the major frequency dependence of the phases. This is true in our case since the frequency range will be limited so that the phase shifts due to P wave propagation and the interface continuity conditions are small compared to those due to S wave propagation. The major interference pattern in $|R|$ will be due to a superposition of the A_o and A_1 waves. The presence of the A_2 wave will add a modulation to this structure.

A typical reflection coefficient to be analyzed is shown in Fig. 11. Four of the maxima and minima are labeled by letters. The basic oscillatory structure is due to the interference of the A_o and A_1 waves. The separation between peaks occurs when ϕ_2 changes by 2π. The difference in

TABLE II

ACOUSTIC PARAMETERS OF THE HOMOGENEOUS SEDIMENT LAYERS

Profile Number	ρ_2 (g/cm^3)	c_z (m/sec)	$k\rho_z$ (dB/m/kHz)	v_2 (m/sec)	k_{s2} (dB/m/kHz)	H (m)
1	1.27	1525	0.115	--	10.0	40
2	1.27	1525	0.115	70	--	40
3	1.27	1525	--	70	10.0	80
4	1.27	--	0.115	70	10.0	100
5	1.27	--	0.115	70	10.0	50
6	--	1525	0.100	100	10.0	50
7	1.25	1525	0.100	100	10.0	50
8	1.25	1525	0.100	100	10.0	50
9	1.25	1525	0.100	100	10.0	50
10	1.25	1525	0.100	100	10.0	50
11	1.25	1525	0.100	100	10.0	50

TABLE III

ACOUSTIC PARAMETERS OF THE SUBSTRATE USED WITH THE HOMOGENEOUS SEDIMENT LAYERS

Profile Number	ρ_3 (g/cm^3)	c_3 (m/sec)	$k\rho_3$ (dB/m/kHz)	v_3 (m/sec)	k_{s3} (dB/m/kHz)
1	2.8	5700	0.152	2900	0.90
2	2.8	5700	0.152	2900	0.90
3	2.8	5700	0.152	2900	0.90
4	2.8	5700	0.152	2900	0.90
5	2.8	5700	0.035	2900	0.07
6	2.8	5700	0.035	2900	0.07
7	2.8	5700	0.035	--	0.07
8	2.8	--	0.035	2900	0.07
9	--	5700	0.035	2900	0.07
10	2.8	5700	0.035	2900	--
11	2.8	5700	--	2900	0.07

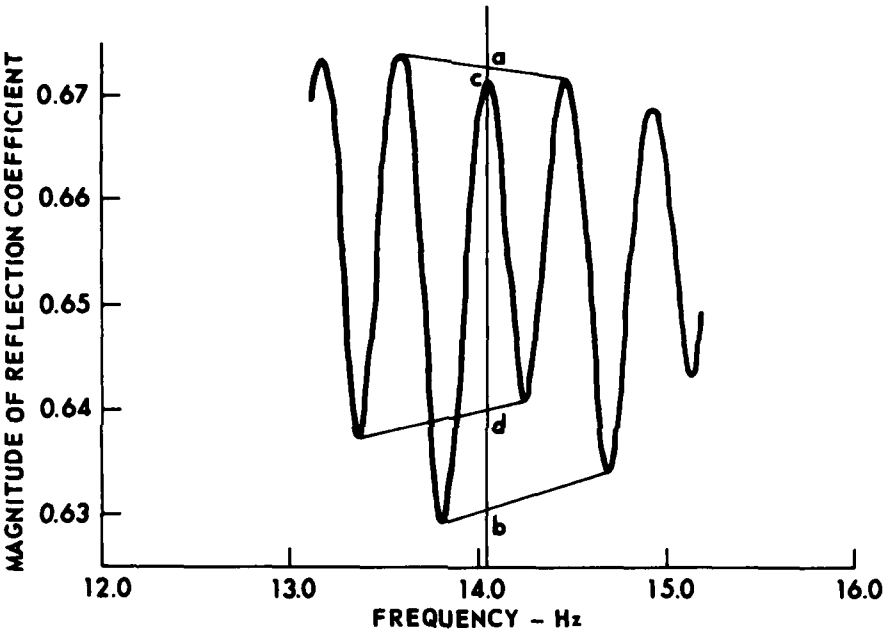

FIGURE 11
EXAMPLE OF THE DEPENDENCE OF THE MAGNITUDE
OF THE REFLECTION COEFFICIENT ON FREQUENCY

ARL:UT
AS-79-1819-P
PJV - GA
8 - 17 - 79

height of peaks b and d clearly shows the effect of the modulation produced by A_2. The unknown amplitudes and the relative phase in Eq. (27) are obtained by setting: $\phi_1=\phi_2=0$ at peak a; $\phi_1=\pi/2$, $\phi_2=\pi$ at valley b; $\phi_1=\pi$, $\phi_2=2\pi$ at peak c; $\phi_1=3\pi/2$, $\phi_2=3\pi$ at valley d. This generates a set of four equations:

$$R_a = A_o + A_1 + A_2 \cos\phi \quad , \tag{28}$$

$$R_b = A_o - A_1 - A_2 \sin\phi \quad , \tag{29}$$

$$R_c = A_o + A_1 - A_2 \cos\phi \quad , \tag{30}$$

$$R_d = A_o - A_1 + A_2 \sin\phi \quad , \tag{31}$$

where R_a, R_b, R_c, and R_d are the measured values of R at a, b, c, and d. These four equations can be easily solved for the four unknowns.

The first parameter to be investigated in the test of the ray model is the sediment shear speed v_2. Profile 1 in Tables II and III was used. Figure 12 shows RL for 3 different shear speeds: 150 m/sec, 70 m/sec, and a fluid case v_2 = 0 m/sec. The results are in qualitative agreement with the ray model predictions. The basic level of RL increases with sediment shear speed. The rapid oscillatory structure, due to the interference of the A_o and A_1 waves, increases in magnitude and spreads out in frequency as v_2 increases. The modulation due to the small A_2 wave is clearly evident in the v_2 = 150 m/sec curve.

Figure 13 shows the dependence of the frequency interval between adjacent maxima of RL, Δf, on sediment shear speed. The line is the ray theory prediction, $\Delta f=v_2/2H$. The agreement is excellent.

Figure 14 shows the dependence of the amplitudes of A_o, A_1, and A_2 waves on sediment shear speed. For reference, v_2 = 150 m/sec corresponds to $\varepsilon\approx0.10$. In agreement with the ray theory predictions, A_1 and A_2 are proportional to v_2 for small shear speeds. The third set

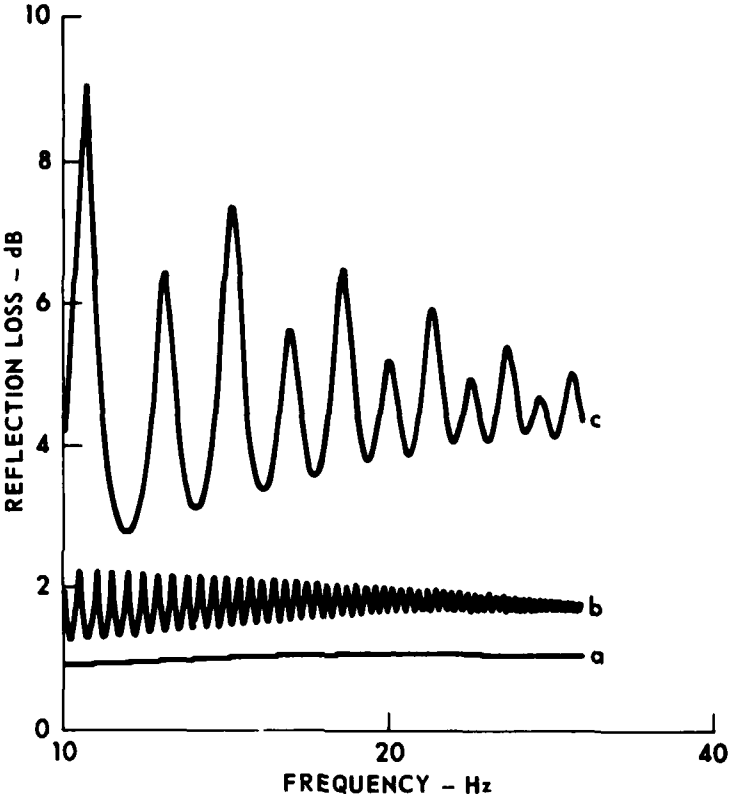

FIGURE 12
REFLECTION LOSS versus FREQUENCY FOR A 40 m THICK HOMOGENEOUS LAYER WITH SEDIMENT SHEAR SPEED AS A PARAMETER
FOR CURVE (a) v_2 0 m/sec; (b) v_2 = 30 m/sec; (c) v_2 = 150 m/sec

ARL:UT
AS-79-1820-P
PJV - GA
8 - 17 - 79

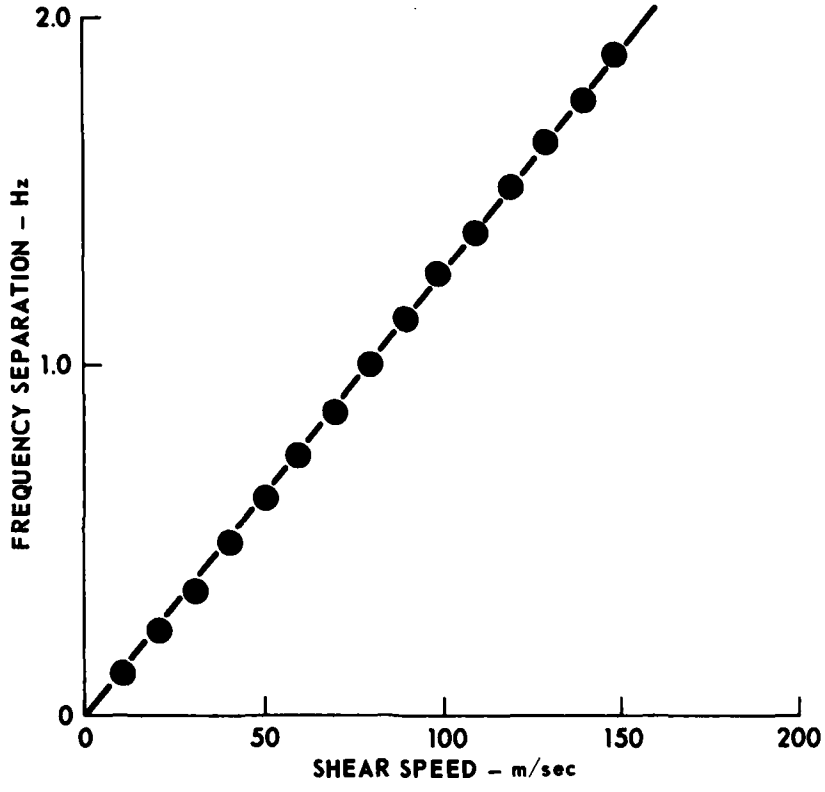

FIGURE 13
THE DEPENDENCE OF THE FREQUENCY INTERVAL
BETWEEN THE ADJACENT MAXIMA OF RL
ON SEDIMENT SHEAR SPEED

ARL:UT
AS-79-1821-P
PJV-GA
8-17-79

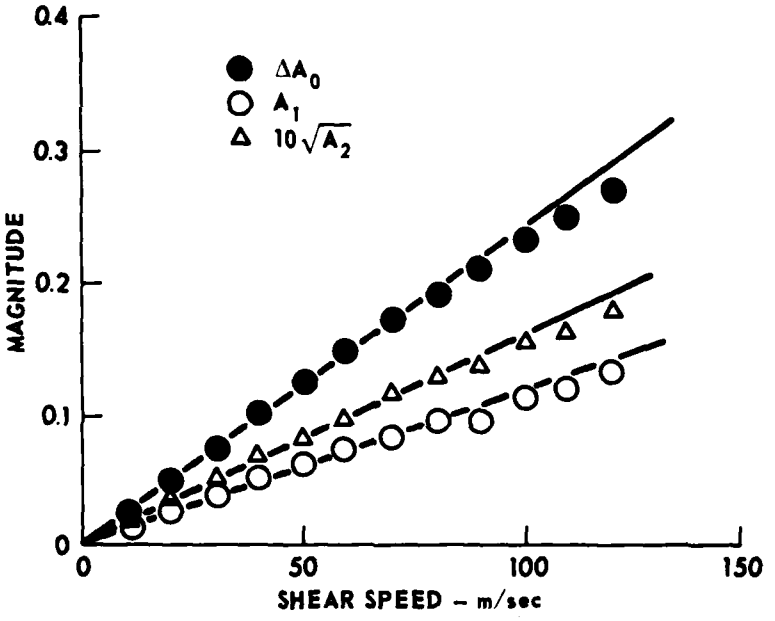

FIGURE 14
THE DEPENDENCE OF THE MAGNITUDES OF THE A_0, A_1, AND A_2 WAVES ON SEDIMENT SHEAR SPEED

ARL:UT
AS-79-1822-P
PJV - GA
8-17-79

of points shows the change of A_o due to sediment rigidity, i.e., $\Delta A_o(\varepsilon) \equiv A_o(0) - A_o(\varepsilon)$. In Fig. 14, A_o increases (RL increases) and is proportional to ε to lowest order, in agreement with the ray theory. The lines in the figure are drawn to illustrate the proportionality to ε. Their slope does not reflect any theoretical prediction. All three sets of points show the effect of higher order corrections at larger ε. The magnitude of A_2 is much smaller than that of A_1, in agreement with the ray theory predictions.

The dependence of A_o, A_1, and A_2 on the sediment shear wave attenuation is shown in Fig. 15. Profile 2 in Tables II and III was used. The earlier discussion of the ray model showed that the magnitude of the A_1 and A_2 waves have different dependencies on the S wave attenuation, i.e., $A_1 \sim \exp(-2k_i H)$ and $A_2 \sim \exp(-k_i H)$, where k_i is the imaginary part of the S wave wave number. The magnitude of the A_o wave is independent of S wave attenuation. The quantity k_s in Fig. 15 is the S wave attenuation in dB/m/kHz. This is related to k_i by $k_i = k_s(f/1000)/8.686$, since we assume a linear dependence of k_i on frequency. The values of k_s greater than 10 attenuate the S wave by 20 dB in a distance 2H. This effectively eliminates any waves other than those shown in Figs. 8 through 10 and permits the ray model to predict a clean exponential dependence on k_s for the magnitudes of the A_1 and A_2 waves. The lines in Fig. 1 are "eyeball" fits to the data obtained from the computed reflection coefficients. The slopes are 0.0285 for the A_2 wave and 0.0569 for the A_1 wave. They differ by a factor of 2 as predicted by the ray theory and agree very well with the predicted slopes of 0.028 and 0.056. The change in A_o due to S waves, ΔA_o, is seen to be independent of k_s as predicted.

The ray model also predicts the dependence of A_1 and A_2 on the magnitude of the sediment P wave after traveling one way through the sediment, $A_2 \sim \exp(-k_i H)$, $A_1 \sim \exp(-2k_i H)$ and $\Delta A_o \sim \exp(-2k_i H)$. For P waves the exponential decay can come from two sources: the attenuation due

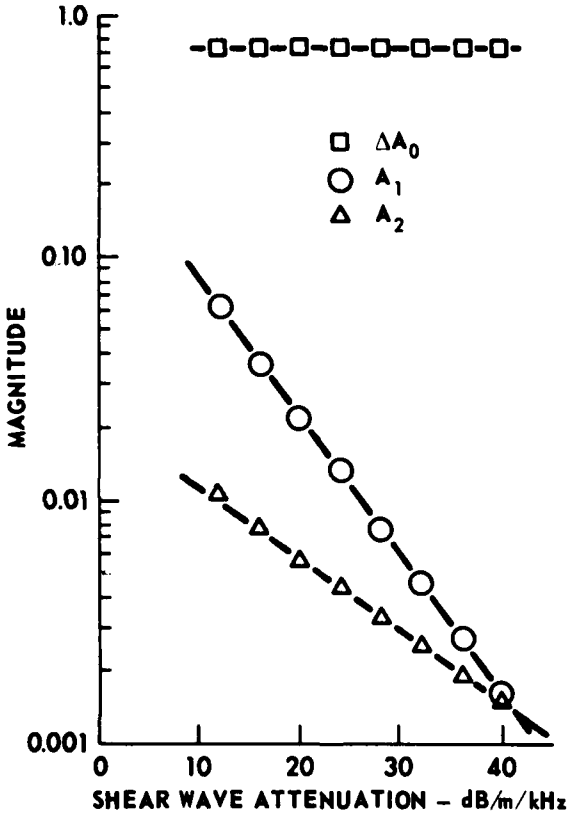

FIGURE 15
THE DEPENDENCE OF THE MAGNITUDES OF THE A_0, A_1, AND A_2 WAVES ON THE ATTENUATION OF THE SEDIMENT SHEAR WAVE

ARL:UT
AS-79-1823-P
PJV - GA
8 - 17 - 79

to traveling through the sediment and also from the evanescent nature of the P wave if the sediment sound speed is larger than that in water. Figure 16, obtained using profile 3 in Tables II and III, shows the dependence of ΔA_o, A_1, and A_2 on k_p, the P wave attenuation in dB/m/kHz. The lines are again "eyeball" fits to the calculated magnitudes. The slopes of the lines are 0.059 for A_2, 0.123 for A_1, and 0.133 for ΔA_o. The A_1 and ΔA_o slopes are nearly double that of the A_2 wave in agreement with the ray model. The values of the slopes also agree well with the predicted values of 0.056 and 0.112. The values of k_p were computed from the actual imaginary part of the wave number, including corrections due to grazing angle.

The ray model strictly predicts no important S wave effects for the cutoff situation, where the sediment P wave speed is larger than the sound speed in water. The incoming ray in the water is specularly reflected with only order ε^2 corrections. The computational model, based on a wave theory, allows the penetration of the P wave into the sediment. It is evanescent and decays exponentially. Generalizing the ray model prediction for the case of P wave attenuation to the case of the evanescent P wave, one obtains the same predictions, with k_i now given by $k_i \approx 2\pi f[(c_2 \cos\phi / c_1)^2 - 1]^{1/2} / c_2$. Since this exponential attenuation is proportional to frequency, it can be written in terms of a frequency independent decay constant k_p', in units of dB/m/kHz, i.e., $k_i = k_p' f / 8686$.

Figure 17 shows the dependence of ΔA_o, A_1, and A_2 on k_p'. The actual parameter varied in this case was the P wave velocity in the sediment. Profile 4 in Tables II and III was used. The lines are "eyeball" fits to the calculated magnitudes. The measured slopes are 0.162 for ΔA_o, 0.162 for A_1, and 0.072 for A_2; the slope of the A_2 line is approximately half that of the slopes of the ΔA_o and A_1 lines in agreement with the ray model predictions. The magnitude of the slopes also agrees well with the predicted values of 0.070 and 0.140.

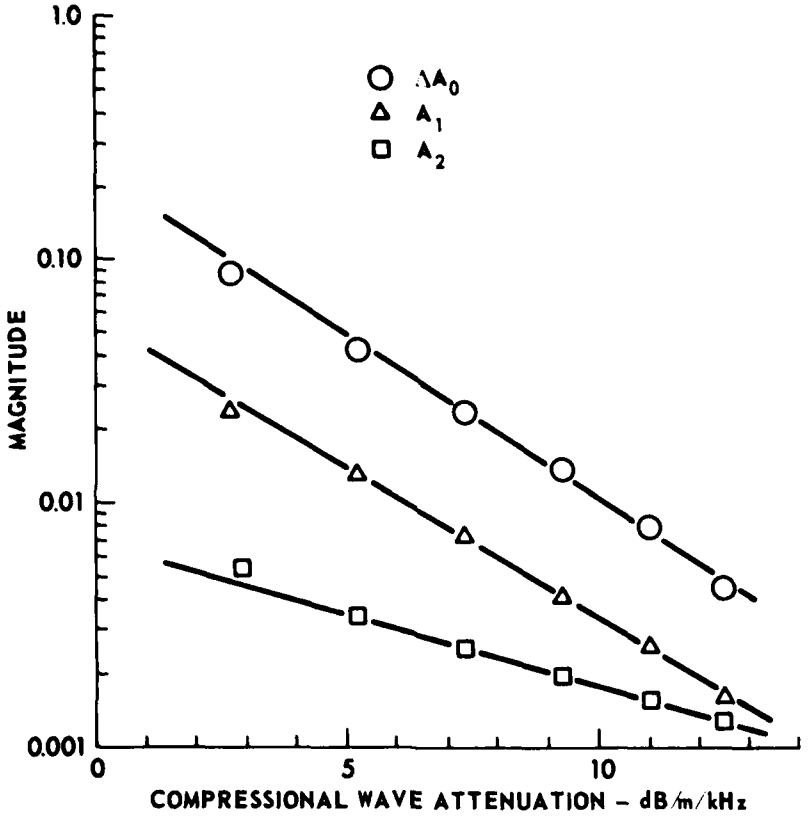

FIGURE 16
THE DEPENDENCE OF THE MAGNITUDES OF THE A_0, A_1, AND A_2 WAVES ON THE ATTENUATION OF THE SEDIMENT COMPRESSIONAL WAVE

ARL:UT
AS-79-1824-P
PJV - GA
8 - 17 - 79

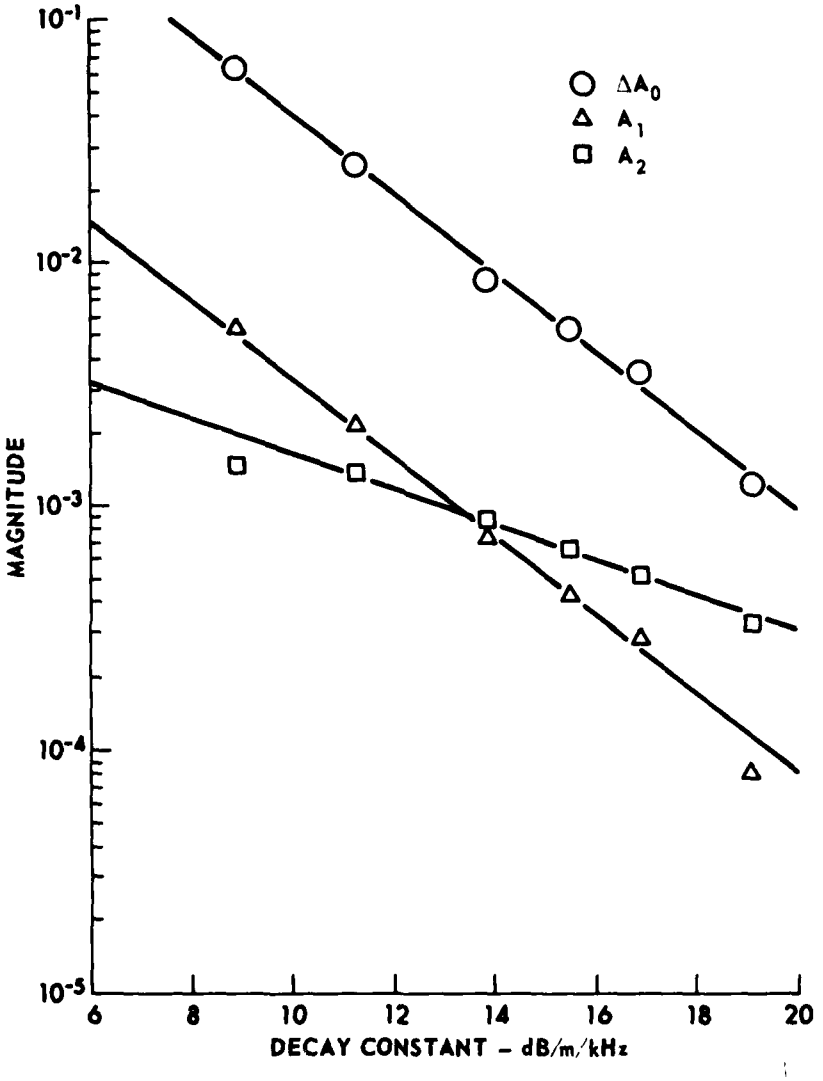

FIGURE 17
THE DEPENDENCE OF THE MAGNITUDES OF THE A_0, A_1, AND A_2 WAVES ON THE ATTENUATION OF THE SEDIMENT COMPRESSIONAL WAVE DUE TO EVANESCENCE

ARL:UT
AS-79-1825-P
PJV - GA
8 - 17 - 79

One of the important conclusions of this paper is that sediment rigidity can be neglected at the water-sediment interface. The ray model supports this conclusion, since it predicts that the lowest order effects depending on the S wave velocity at the W/S interface are contained in the ϵ_u^2 and $\epsilon_u\epsilon_L$ waves seen in Fig. 9. Since $\epsilon \leq 0.1$, these are small corrections compared to the ϵ_L corrections seen in Figs. 8 and 10 due to P wave conversion at the S/S interface.

Figure 18 illustrates the relative insensitivity of R to the sediment S wave velocity at the W/S interface (v_{2u}) compared to that at the S/S interface (v_{2L}). Figures 18(a) and 18(b) use the computational model to follow the development of $|R|$, starting with a homogeneous layer in which v_2 = 100 m/sec and ending with v_2 = 300 m/sec. To eliminate interference effects, a frequency in the high frequency regime was chosen. In Fig. 18(a) v_{2u} is constant while v_{2L} increases. A constant gradient is used which has the value of 5/sec when v_{2L} = 300 m/sec. Three grazing angles are shown. $|R|$ decreases almost linearly with v_{2L} at each grazing angle. The decrease is significant, 30% at θ=30° and 50% at θ=10°. Figure 18(b) shows the additional change in $|R|$ which occurs when v_{2L} is held constant at 300 m/sec and v_{2u} increased to form a homogeneous layer with v_2 = 300 m/sec. As expected, the factor of three change in v_{2L} now produces only small changes in $|R|$. Compared to $|R|$ for the original 100 m/sec homogeneous layer, the changes are 1.6% at θ=10° and 4% at θ=30°. These are small changes compared to those produced by changing v_{2L}. This result reinforces the conclusion that RL is relatively insensitive to the surficial S wave velocity. In fact, fairly accurate values of $|R|$ can be obtained in the high frequency regime by assuming a homogeneous layer with v_2 given by the S wave velocity at the sediment-substrate interface. For the same gradients used in Fig. 18(a) the error produced by this assumption is less than 12% over the entire range of gradients and for grazing angles less than 50°. This leads to the conclusion that v_{2L} is the important S wave parameter in the high frequency regime; gradients and v_{2u} are not major factors influencing RL.

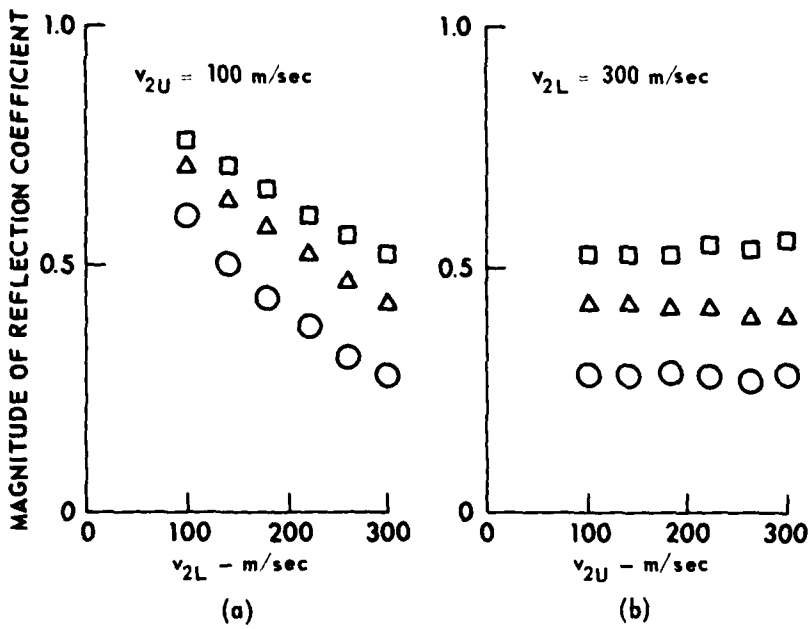

FIGURE 18
THE DEPENDENCE OF THE MAGNITUDE OF THE REFLECTION COEFFICIENT ON THE SEDIMENT SHEAR WAVE SPEED AT INTERFACES FOR GRAZING ANGLES OF 10° (CIRCLES), 20° (TRIANGLES), AND 30° (SQUARES)

ARL:UT
AS-79-1826-P
PJV - GA
8 - 17 - 79

IV. PARAMETER STUDIES

In this section the effect of bottom parameter variations on the bottom reflection loss of a solid sediment will be studied. The computational model will be used to obtain R. The study will be restricted to thin sediment layers for which sediment rigidity is important. Current geophysical data will be used to limit the parameter ranges. We first consider homogeneous layers and use the amplitudes of the interfering waves in the ray picture (A_o, A_1, A_2) to quantify the changes in RL due to sediment S wave propagation. Next we treat layers with gradients, using mainly the change in RL to identify significant parameters. Finally, the question of the accuracy required in sediment parameter values to accurately predict RL is addressed. This is done by varying the parameters of a typical deep sea sediment.

A. Homogeneous Layers

The ray picture presented earlier shows that RL is due to the interference between the A_o, A_1, and A_2 waves. The interference structure can be quite strong at low frequencies where sediment S wave attenuation is small. At high frequencies the increased S wave attenuation effectively eliminates the A_1 and A_2 waves and destroys the interference pattern. The A_o wave remains to carry the effects of sediment rigidity at high frequencies. The A_o wave also carries the effects due to a fluid sediment. The difference ΔA_o between the A_o wave for fluid and solid sediments is entirely due to sediment rigidity.

In this section the results of our study of the influence of parameter variations in a homogeneous sediment layer on ΔA_o, A_1, and A_2 will be presented. In these studies the grazing angle was held at 20°, and the wave magnitudes were obtained at a frequency of 14 Hz. The changes produced by variations of a single parameter, over the range given by geophysical data, will be presented. The bottom structure is given in Tables II and I'I: Table II gives sediment

parameters, and Table III gives substrate parameters. In all cases the sound speed in water was taken to be 1540 m/sec and the water density to be 1.053 g/cm^3. First, the effect of parameter variation on ΔA_o will be discussed; its behavior will hold in both high and low frequency regimes. Next, we will discuss the behavior of the A_1 and A_2 waves which are important in the low frequency regime. Three categories of parameters will emerge: those that are definitely important, those which can be neglected, and those which are important under certain conditions. The criterion used is that a parameter is important if it produces a change of 10% when varied over half the possible range of variation given by geophysical data. The parameter ranges are given in Table IV. We restrict ourselves to high porosity, deep sea sediments for which our computational model applies. The profiles, from Tables II and III, used in each study are also given in Table IV.

As expected from the ray picture and the expansion theory of the reflection and transmission coefficients, the sediment shear speed greatly affects ΔA_o. Not only is a finite shear speed necessary to describe thin sediments, but changing it by 50 m/sec produces a 50% increase in ΔA_o. Surprisingly, the only other important parameters are the sediment P wave speed and density. This is surprising since for the corresponding fluid sediments we find that the variation of these parameters produces very small changes in RL (<4%). For the solid sediment case, a change in P wave speed of 80 m/sec produced 50% changes in ΔA_o and a change of 0.25 g/cm^3 in sediment density changed ΔA_o by about 15%.

In the category of negligible parameters for ΔA_o are substrate density and substrate P and S wave attenuations. These parameters only enter through the boundary conditions at the sediment-substrate interface. The negligible effect of the attenuations is reasonable since they are only a small part of the total complex wave velocities. Sediment P wave attenuation can also be ignored. This is due to the low frequency, and to sediment thickness.

TABLE IV

ACOUSTIC PARAMETER RANGES, PROFILE NUMBERS IN TABLES II AND III USED IN PARAMETER STUDIES, AND REFERENCE NUMBERS

Parameter	Range	Profile Number	Reference
v_2 m/sec	50-150	1	10
k_{s2} dB/m/kHz	8.7-26.1	2	11
k_2 dB/m/kHz	0-0.2	3	18
c_2 m/sec	1500-1620	4,5	19
ρ_2 g/cm^3	1.1-1.6	6	20
v_3 m/sec	1700-3600	7	21
c_3 m/sec	3500-6700	8	21
ρ_3 g/cm^3	2.1-3.0	9	21
k_{s3} dB/m/kHz	0.06-0.50	10	11
k_{p3} dB/m/kHz	0.02-0.05	11	18

The category of conditionally important parameters for ΔA_o contains the sediment S wave attenuation and the substrate P and S wave velocities. As expected from Fig. 15, varying the shear wave attenuation over most of its range has an insignificant effect on ΔA_o. Only for very low values of k_{s2} is ΔA_o affected. This is probably due to the extreme interference effects for small k_{s2} producing many order ϵ^1 rays, which then combine into an order ϵ^o contribution. These additional contributions would not have the expected ϵ scaling and would appear as part of ΔA_o in our analysis of $|R|$. The effect of substrate compressional speed on ΔA_o is shown in Fig. 19. For large c_3, between 5000 and 6600 m/sec, the change in ΔA_o is about 10%. For small c_3, between 3400 and 5000 m/sec, the change in ΔA_o is significant, particularly at the lower values. The substrate P wave speed is then a significant parameter for small values, but is negligible if its value is large enough. The same is true of the substrate S wave speed, the separation between the two regimes being at 2600 m/sec.

One additional parameter is the sediment thickness. For homogeneous layers the differential equations for sediment P and S waves can be written in terms of scaled depth $Z=z/H$, where z is the depth below the water-sediment interface. The complex wave velocities are then scaled to the velocity $V=\omega H$. The interface continuity conditions can also be written in terms of the same velocity, V. This means that for homogeneous layers the frequency and depth enter only through the parameter V. The dependence of RL on depth is then the same as the dependence on frequency. In fact, RL obtained for $\omega=\alpha\omega_o$ and $H=H_o$ is the same as that for $\omega=\omega_o$ and $H=\alpha H_o$, i.e., increasing the frequency is the same as increasing the layer thickness. This relation between ω and H will hold only approximately for layers with gradients. In this case there are additional scale lengths in the problem, those associated with the gradients which prevent the differential equations from being scaled.

The dependence of A_1 and A_2 on the bottom parameters has a slightly different structure. The sediment density shifts from being an important parameter to being a negligible parameter whereas the sediment S wave

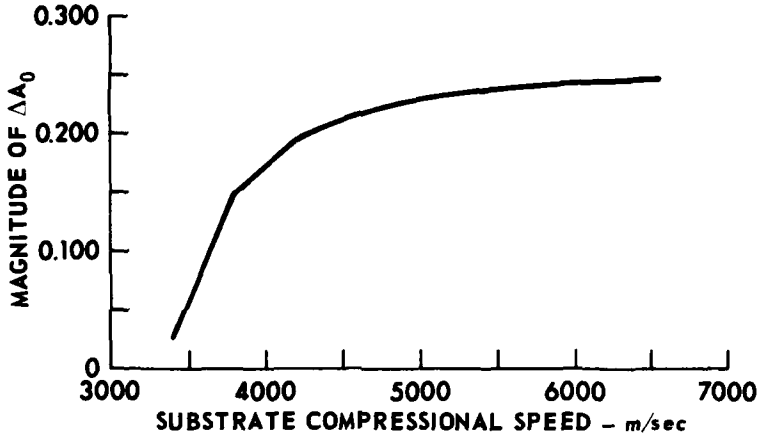

FIGURE 19
THE DEPENDENCE OF ΔA_0 ON THE SUBSTRATE COMPRESSIONAL WAVE SPEED

ARL:UT
AS-79-1827-P
PJV- GA
8-17-79

attenuation shifts from the conditional to important category. All other parameters stay in the same categories.

B. Layers with Gradients

This section presents the effect of parameter gradients on RL of a solid, deep sea sediment. This study of gradient effects is accomplished by allowing one parameter at a time to have a gradient in an otherwise homogeneous layer. The parameters of the homogeneous layer are typical of deep sea sediments. Using the subscript convention of the expansion theory above, the parameters are $\rho_1 = 1.053$ g/cm^3, $c_1 = 1540$ m/sec, $\rho_2 = 1.25$ g/cm^3, $c_2 = 1525$ m/sec, $k_{p2} = 0.100$ dB/m/kHz, $v_2 = 100$ m/sec, $k_{s2} = 10.0$ dB/m/kHz, $\rho_3 = 2.8$ g/cm^3, $c_3 = 5700$ m/sec, $k_{p3} = 0.035$ dB/m/kHz, $v_3 = 2900$ m/sec, and $k_{s3} = 0.070$ dB/m/kHz. The layer thickness is H = 40 m. The effect of gradients on the high frequency regime was obtained by examining the change in RL as a function of grazing angle with the gradient as a parameter at a fixed frequency (50 Hz). The effect on the low frequency interference regime was obtained in a similar manner, with the frequency chosen to be one of the peaks in RL. For most parameters this frequency is 19.45 Hz. For the case of the gradient in sediment S wave velocity the frequency was chosen for each gradient to be the largest interference peak near the original frequency of 19.45 Hz. This frequency depends on the gradient since the shear wave phase accumulated in traveling through the sediment depends on the actual gradient.

The first parameter to be discussed is the S wave speed. Typical gradients of v_2 are expected to be about 4.65 sec^{-1} (Ref. 10). Figures 20 and 21 show the effect of the gradient of S wave speed on RL. At 50 Hz (Fig. 20), the high frequency regime, RL increases steadily with increasing gradient. This is the result to be expected from the ray picture. The major effect of the gradient at high frequencies is to increase the S wave speed at the lower interface, thus increasing the sediment S wave amplitude. The increase is quite large

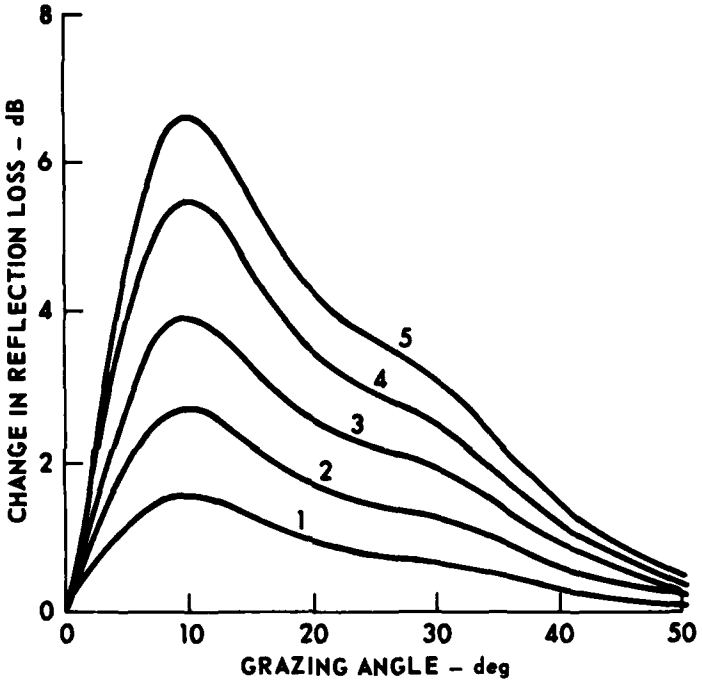

FIGURE 20
THE CHANGE IN REFLECTION LOSS
versus GRAZING ANGLE AT 50 Hz
WITH SHEAR SPEED GRADIENT (IN UNITS
OF sec^{-1}) AS PARAMETER

ARL:UT
AS-79-1828-P
PJV - GA
8 - 17 - 79

with a peak of 6.2 dB at 10°, and decreases at both higher and lower grazing angles. At low frequencies, where S wave propagation is important, the structure of large peaks (Fig. 5) changes with the gradient of S wave speed. The separation between peaks increases from 0.65 Hz for the homogeneous layer to 1.10 Hz for a gradient of 5 sec^{-1}. In addition, Fig. 21 shows that the magnitude of the interference effect also increases for larger gradients. The magnitude of the increase in RL is only about 1 dB larger than that for the high frequency regime of Fig. 20. The increase with gradient is not as regular as that in Fig. 20. These changes can be qualitatively explained by the ray picture. The basic effect of the gradient on the change in RL occurs through the increase of S wave speed at the sediment-substrate interface. The magnitude of ΔA_L will increase in the same manner in both high and low frequency regimes, and thus the major part of the increase in RL in both frequency regimes is accounted for. The more erratic increases at low frequencies (Fig. 21) are probably due to the combination of higher order corrections to the reflection and transmission coefficients (ε_L = 0.2 at a gradient of 5) and the phase shift between the A_1 and A_2 waves.

The effect of the depth dependence of the S wave attenuation is shown in Fig. 22. The frequency is 19.45 Hz, which corresponds to a maximum in RL at θ=20°. The depth dependence was calculated by assuming that the ratio between the logarithmic decrements (ratio of the imaginary part of the wave numbers to the real part) of shear and compressional waves is constant with depth. At the sediment surface this ratio is typically Δ_s/Δ_p=0.3 for deep sea sediments.[11] Converting to attenuation gives $k_{s2}(z)=k_{p2}(z)[c_2(z)/v_2(z)]\Delta_{s2}/\Delta_{p2}$. The major depth dependence occurs because of the increase of S wave speed v_2 with depth, resulting in a decrease in attenuation with depth. Approximating this depth dependence by a constant gradient and using parameters typical of deep sea sediments[10,19] gives $dk_{s2}/d_z \simeq -0.15$ dB/m^2/kHz. Figure 22

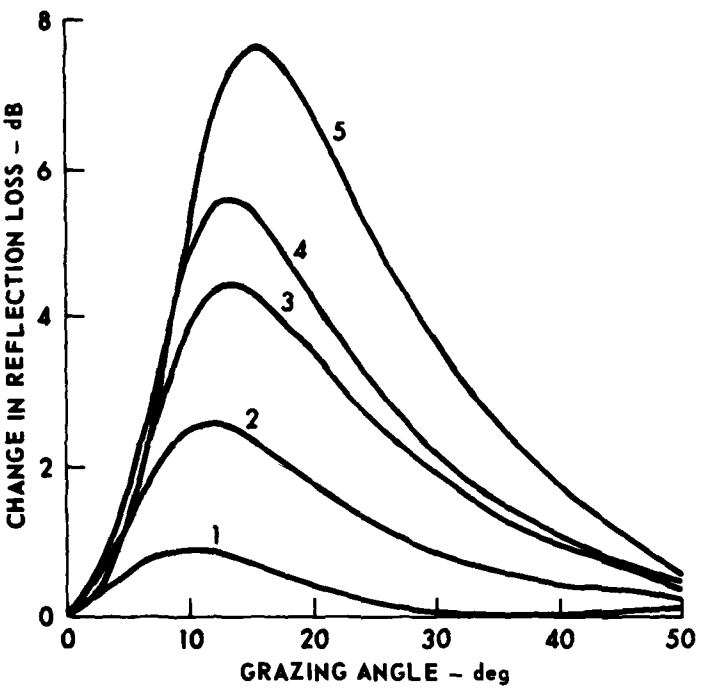

FIGURE 21
THE CHANGE IN REFLECTION LOSS
versus GRAZING ANGLE AT 19.45 Hz
SHEAR SPEED GRADIENT (IN UNITS
OF sec^{-1}) AS PARAMETER

ARL:UT
AS-79-1829-P
PJV- GA
8-17-79

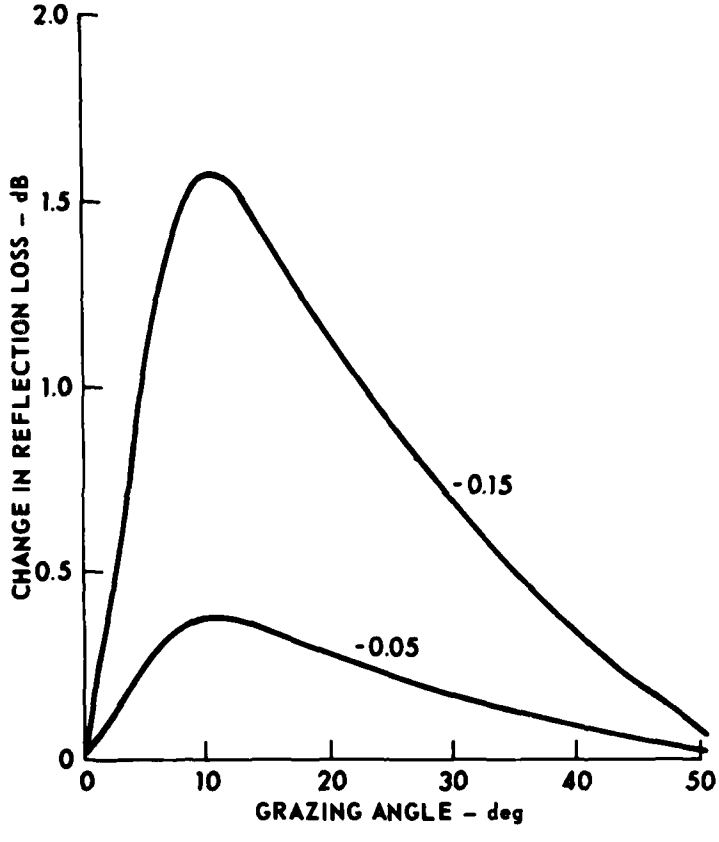

FIGURE 22
THE CHANGE IN REFLECTION LOSS
versus GRAZING ANGLE AT 19.45 Hz
THE GRADIENT OF SHEAR WAVE ATTENUATION
(IN UNITS OF $dB/m^2/kHz$) AS PARAMETER

ARL:UT
AS-79-1830-P
PJV - GA
8 - 17 - 79

shows that this decrease in S wave attenuation produces a significant change in RL in the low frequency regime. This is expected since a decrease in attenuation will increase the effectiveness of interference effects. In the high frequency regime the gradient in S wave attenuation produces insignificant (0.15 dB) changes in RL. This also is expected since in the high frequency regime the S waves are completely absorbed within the sediment. The change in total attenuation produced by the attenuation gradient is too small to keep the S wave from being absorbed. The effect of the gradient could at most increase the frequency characterizing the separation of the high and low frequency regimes.

Typical gradients in density[20] (<0.000025 g/cm^3/m) and P wave attenuation[18] ($\sim 2.5\times10^{-4}$ dB/kHz/m^2) produced negligible (<0.05 dB) changes in RL at low grazing angles (0 to 50°).

To study the effect of the gradient in P wave speed it was necessary to remove the excitation of Stoneley waves at the sediment-substrate interface. This was done by changing the substrate parameters to $\rho_3 = 2.6$ g/cm^3, $c_2 = 4900$ m/sec, $v_2 = 2400$ m/sec. The changes in RL shown in Figs. 23 and 24 are then due to the gradient alone and are not related to the excitation of interface waves. Gradients of P wave velocity are typically[22] less than 2 sec^{-1}.

Figures 23 and 24 show that RL is a solid sediment surprisingly sensitive to the gradient of P wave speed. At low frequencies (Fig. 23) an increase of over 4 dB was observed at low grazing angles for a gradient of 2 sec^{-1}. The increase in RL is even larger in the high frequency regime. Figure 24 shows an increase of nearly 10 dB. The gradient in P wave speed is clearly an important sediment parameter.

C. Sensitivity of RL to Parameter Accuracy

In this section we investigate the question of how a small change in an ocean bottom parameter influences the bottom reflection loss. This

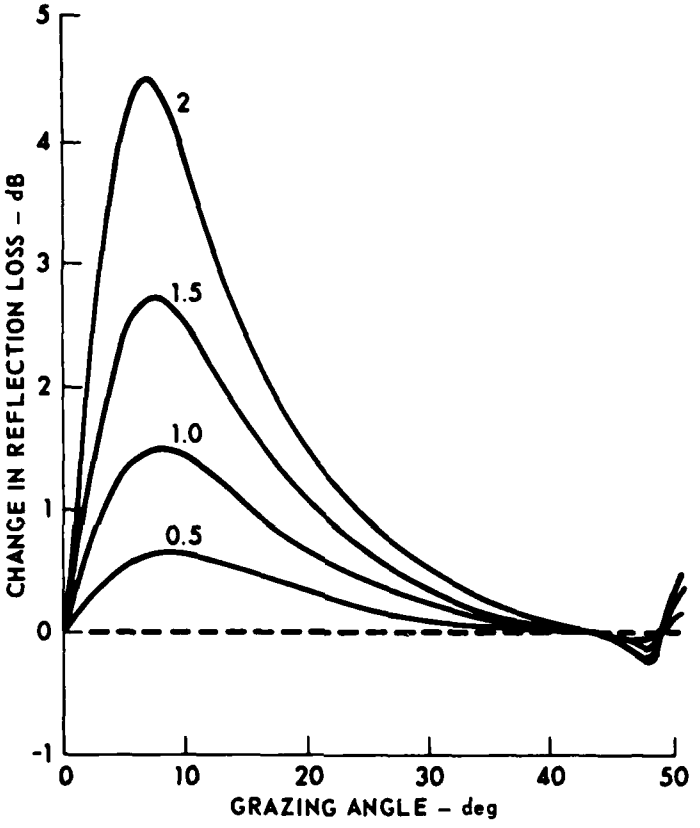

FIGURE 23
THE CHANGE IN REFLECTION LOSS
versus GRAZING ANGLE AT 19.45 Hz
THE GRADIENT OF THE COMPRESSIONAL WAVE
SPEED (UNITS OF sec^{-1}) AS PARAMETER

ARL:UT
AS-79-1831-P
PJV - GA
8 - 17 - 79

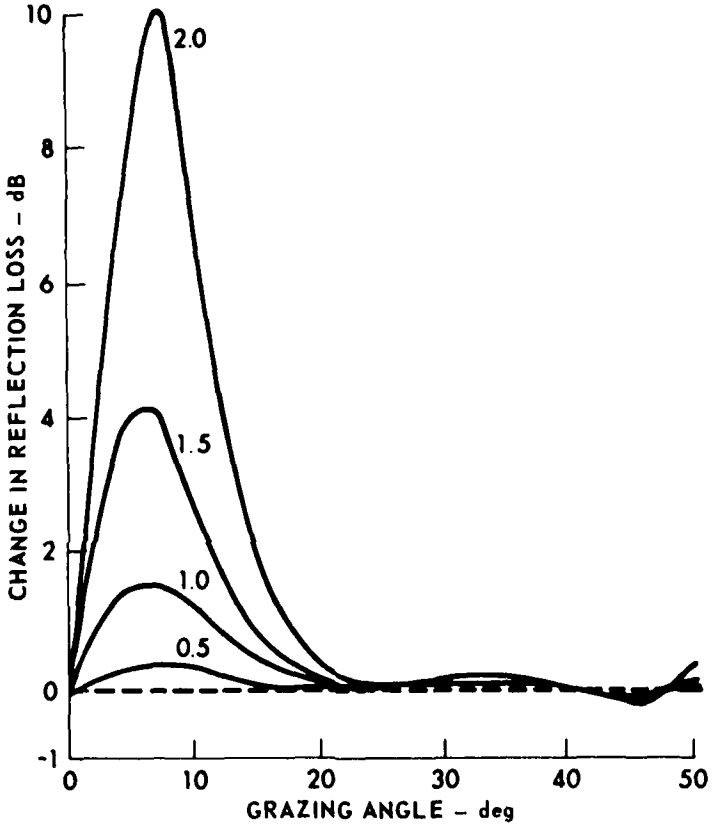

FIGURE 24
THE CHANGE IN REFLECTION LOSS
versus GRAZING ANGLE AT 50 Hz
THE GRADIENT OF THE COMPRESSIONAL WAVE
SPEED (UNITS OF sec^{-1}) AS PARAMETER

ARL:UT
AS-79-1832-P
PJV - GA
8 - 17 - 79

is done by perturbing the parameters of a thin sediment layer having realistic parameters and computing the resulting change in RL. Parameters will be varied one at a time so that their effects can be isolated. Parameters will be grouped into three categories: high sensitivity, normal sensitivity, and low sensitivity. For high sensitivity parameters the fractional change in RL will be greater than the fractional change in the parameter. Normal sensitivity parameters will induce changes in RL of the same size or slightly less than the fractional change in the parameter. Low sensitivity parameters will induce a change in RL an order of magnitude or more smaller than the change in the parameter. Low grazing angles and the high frequency regime will be treated.

The parameters of the layer studied are given in Table V. They were obtained from the geophysical literature and are typical of high porosity, deep sea sediment types. Figure 25 shows the RL for 0 to 45° grazing angles in the high frequency regime at 50 Hz. This figure provides a reference level to put the change in RL induced by parameter variations into perspective. The expected increase in RL due to sediment rigidity (~5 dB) is seen. Bottom parameters will be changed by ±10% about the nominal values of Table V. Parameters were put into the high sensitivity category if they induced a change in RL of more than 20% (about 2 dB). If the change was less than 5% (about 0.4 dB), they were put into the low sensitivity category. The normal category contained parameters inducing changes in RL of between 5% and 20%, about the same size as the parameter change.

The low sensitivity category contained all attenuations and their gradients as well as the gradients of sediment density and P wave velocity. The sediment surficial S wave speed is, surprisingly, also a low sensitivity parameter. All were varied by ±10%. In order of decreasing sensitivity they were: v_2(0.30 dB), k_{p2}(0.15 dB), c_2'(0.08 dB), k_{s2}(0.06 dB), ρ_2'(0.03 dB), k_{s2}'(0.02 dB), and k_{s3}, k_{p3}, k_{p2}' (all inducing changes of less than 0.01 dB). The prime denoted the derivative with respect to depth.

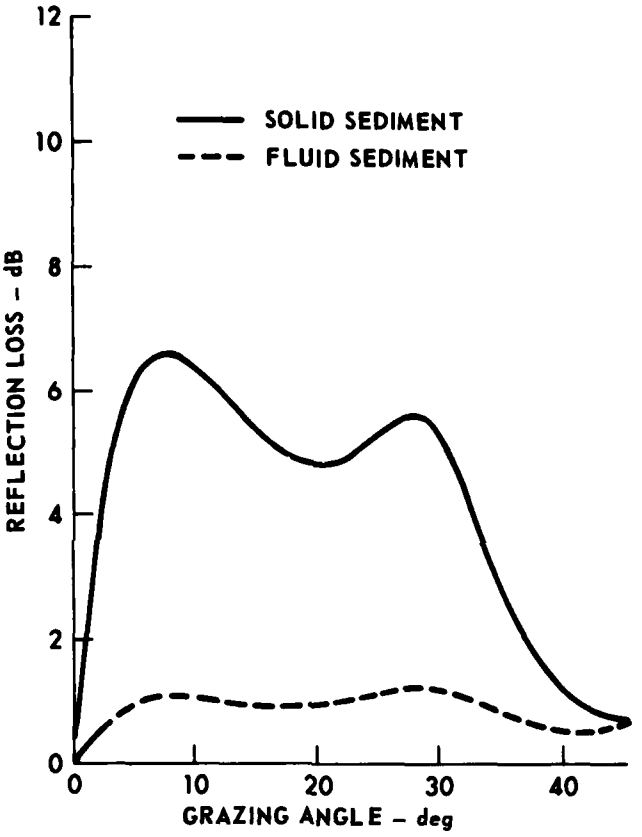

FIGURE 25
REFLECTION LOSS versus GRAZING ANGLE
FOR A TYPICAL DEEP-SEA SEDIMENT LAYER
40 m THICK AT 50 Hz

ARL:UT
AS-79-1833-P
PJV - GA
8 - 17 - 79

TABLE V

ACOUSTIC PARAMETERS OF THE OCEAN BOTTOM USED TO STUDY THE SENSITIVITY OF REFLECTION LOSS TO PARAMETER ACCURACY. CONSTANT GRADIENTS ARE ASSUMED.

Depth (m)	c (m/sec)	b_p (dB/m/kHz)	ρ (g/cm^3)	v (m/sec)	k_s (dB/m/kHz)
water	1530	--	1.03	--	--
0	1511	0.115	1.530	116	15.00
40	1563	0.125	1.586	302	9.00
Substrate	4930	0.030	2.600	2460	0.030

Normal sensitivity parameters in order of decreasing sensitivity were found to be: H(1.7 dB), ρ_2(1.5 dB), ρ_3(0.76 dB), c_3(0.68 dB), ρ_1(0.13 dB for 2% change), and v_2'(0.45 dB). The sediment S wave velocity gradient appears in this group. The rather large changes induced by ρ_3 and c_3 indicate the importance of the substrate interface. The effect of changing the sediment thickness by ±10% is seen in Fig. 26. The large peaks between 20° and 30° are the result of changes in the level of RL and are not due to a shift in the RL curve with angle. Figure 27 shows the effect of changing the sediment surficial density by ±10%. The induced changes are also concentrated at low grazing angles.

The high sensitivity parameters are c_1, c_2, and v_3. Varying the sound speed in water by ±1% induced the change in RL shown in Fig. 28. The change in RL for -1% is nearly the mirror image of that for +1%. The changes are most important at very low grazing angles (~5°) and are small above 15°. Inspection of the RL versus θ curve shows that the changes near 5° are not due to a slight shift in angle of the rapidly increasing RL at low angles, but rather are due to an actual change in RL. The change in RL induced by changing c_2 by ±10% is shown in Fig. 29. The corresponding changes for a fluid sediment are also shown. The changes are not symmetric for ±10% changes in c_2. For the solid sediment RL decreases quite substantially at small angles. For the fluid sediment case the changes are much smaller except that the large peak occurs near 20° in the +10% case; this peak is due to the excitation of a Stoneley wave at the substrate interface by the evanescent P wave in the sediment. Note that this does not occur in the solid sediment case, i.e., sediment rigidity greatly reduces the coupling into interface waves at the substrate interface. The very large sensitivity to c_1 is reduced substantially if the ratio c_2/c_1 is held constant. Varying c_1 (and hence c_2) by 1% then produces changes of at most 0.28 dB, an order of magnitude smaller than the 2.7 dB change seen in Fig. 28. The effect of varying substrate S wave velocity is given in Fig. 30. The changes are nearly symmetric for ±10% changes. The large increase near 45° is

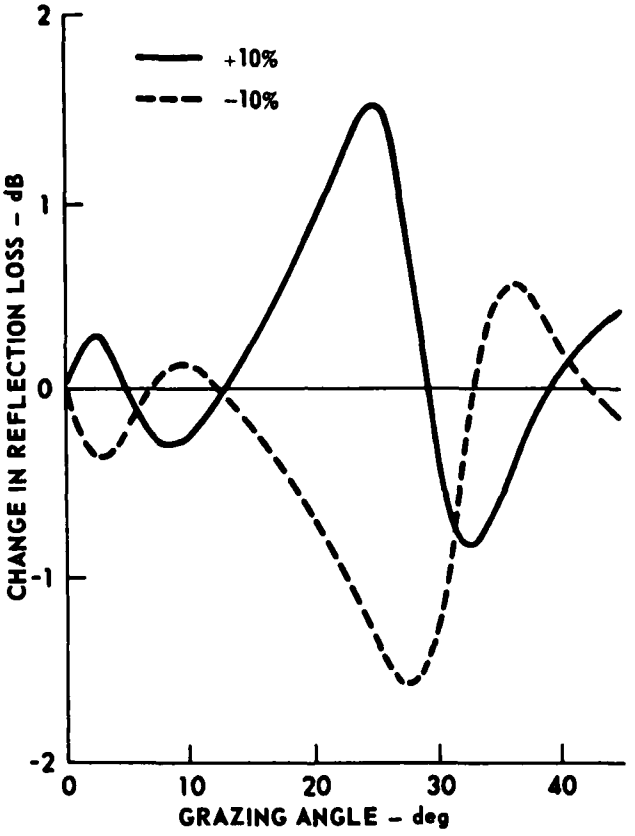

FIGURE 26
THE CHANGE IN REFLECTION LOSS versus GRAZING ANGLE FOR ±10% CHANGES IN LAYER THICKNESS

ARL:UT
AS-79-1834-P
PJV - GA
8 - 17 - 79

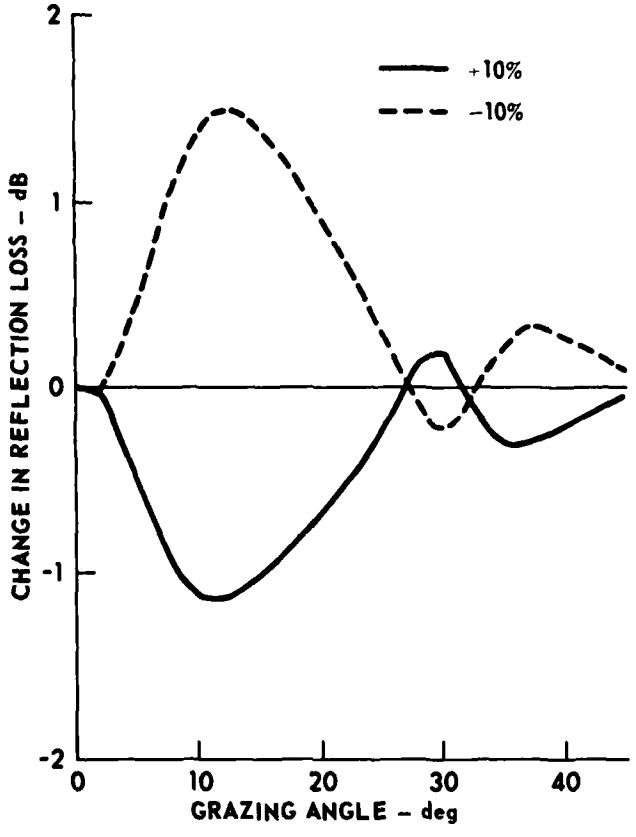

FIGURE 27
THE CHANGE IN REFLECTION LOSS versus
GRAZING ANGLE FOR ±10% CHANGES
IN SURFICIAL SEDIMENT DENSITY

ARL:UT
AS-79-1835-P
PJV-GA
8-17-79

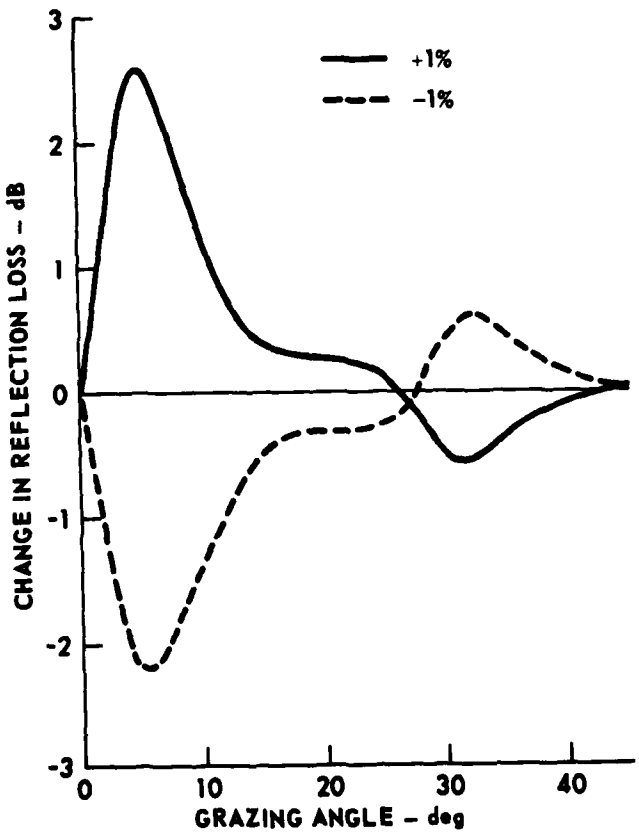

FIGURE 28
THE CHANGE IN REFLECTION LOSS versus
GRAZING ANGLE FOR ±1% CHANGES
IN THE SOUND SPEED IN WATER

ARL:UT
AS-79-1836-P
PJV-GA
8-17-79

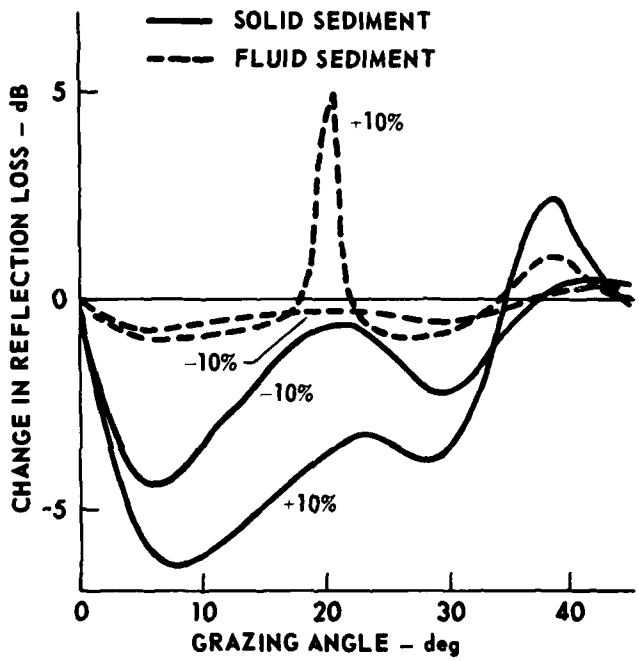

FIGURE 29
THE CHANGE IN REFLECTION LOSS versus GRAZING ANGLE FOR ±10% CHANGES IN THE SURFICIAL COMPRESSIONAL WAVE SPEED IN THE SEDIMENT

ARL:UT
AS-79-1837-P
PJV - GA
8 - 17 - 79

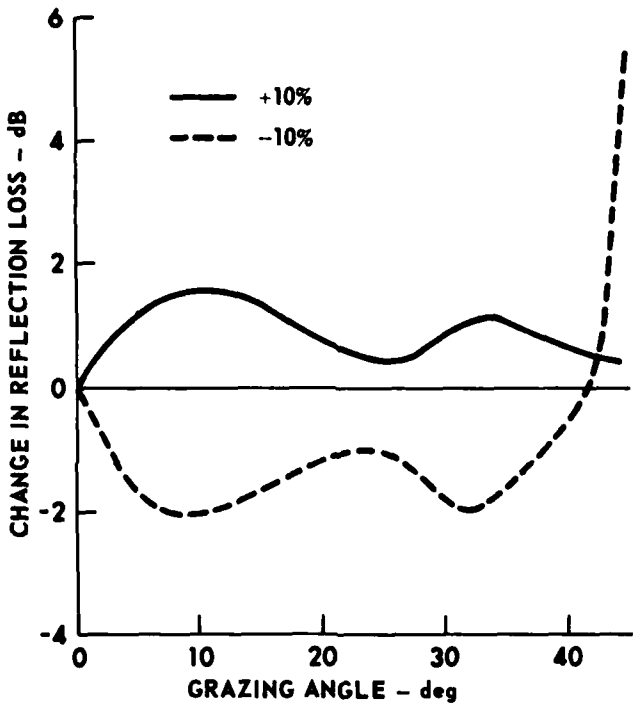

FIGURE 30
THE CHANGE IN REFLECTION LOSS versus
GRAZING ANGLE FOR ±10% CHANGES
IN THE SUBSTRATE SHEAR SPEED

ARL:UT
AS-79-1838-P
PJV - GA
8 - 17 - 79

due to a slight shift, to lower grazing angles, of the rapidly increasing RL near 50° due to substrate shear wave excitation near its critical angle.

D. Additional Topics

Two final topics are considered in this section. First is the effect of sediment rigidity on the excitation of interface waves on the sediment-substrate interface. For the case of a fluid sediment, Stoneley waves traveling along the substrate interface have been identified as a possible loss mechanism at low grazing angles, producing very large RL over a very small interval of grazing angles. The characteristics of these interface waves for fluid sediments have been studied in detail.[5,6] The last topic is a discussion of sediment rigidity effects in sands, an important sediment type in shallow water, continental shelf areas.

The bottom parameters used in the study of sediment rigidity on RL were taken from the work of Hawker[5] so that the Stoneley wave peak in RL for the fluid sediment case could be unambiguously identified. The parameters of the water column are: $\rho_1 = 1.053$ g/cm^3, $c_1 = 1540$ m/sec. The sediment layer is 100 m thick. Sediment parameters at the water-sediment interface are: $\rho_2 = 1.27$ g/cm^3, $c_2 = 1527$ m/sec, $k_{p2} = 0.057$ dB/m/kHz, $k_{s2} = 8.0$ dB/m/kHz. The sediment shear wave speed was varied to determine the effect of sediment rigidity. A homogeneous layer was assumed except for a constant sound speed gradient, $dc_2/dz = 1.2$ sec^{-1}. The substrate parameters are: $\rho_3 = 2.6$ g/cm^3, $c_3 = 5700$ m/sec, $k_{p3} = 0.03$ dB/m/kHz, $v_3 = 2900$ m/sec, $k_{s3} = 0.030$ dB/m/kHz.

Figures 31 through 33 show the effect of sediment rigidity on interface wave excitation at frequencies of 25, 50, and 100 Hz, respectively. The dashed curves were obtained for the fluid sediment case. The peaks in RL near 18° are due to Stoneley wave excitation. The solid curves in each figure show the effect of sediment rigidity for $v_2 = 100$, 200, and 400 m/sec. A value of 400 m/sec is typical at a depth of 100 m for a clay sediment.

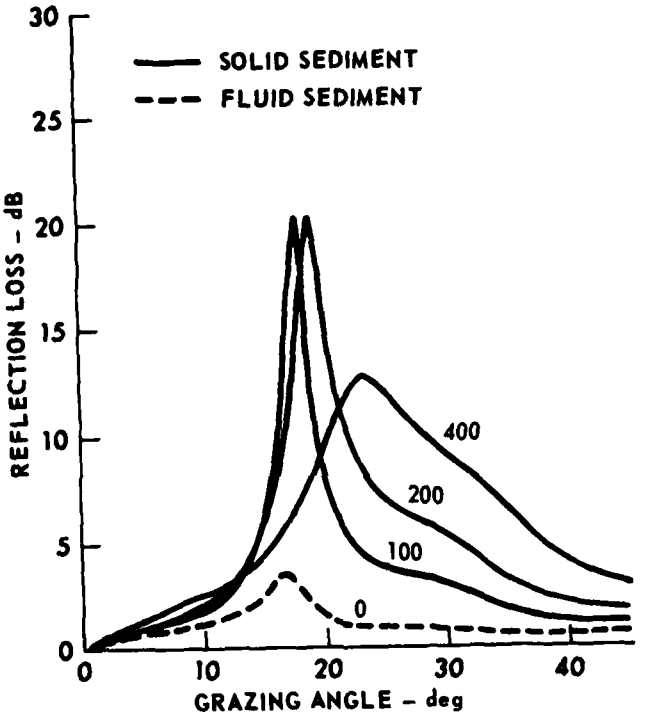

FIGURE 31
REFLECTION LOSS versus GRAZING ANGLE
FOR A 100 m THICK CLAY LAYER AT 25 Hz
THE PARAMETER IS THE SEDIMENT SHEAR
WAVE SPEED IN UNITS OF m/sec

ARL:UT
AS-79-1839-P
PJV-GA
8-17-79

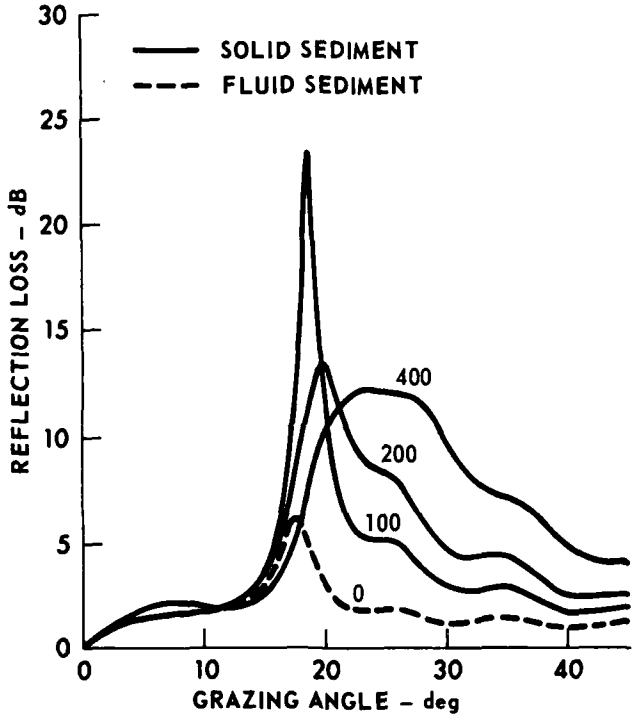

FIGURE 32
REFLECTION LOSS versus GRAZING ANGLE
FOR A 100 m THICK CLAY LAYER AT 50 Hz
THE PARAMETER IS THE SEDIMENT SHEAR
WAVE SPEED IN UNITS OF m/sec

ARL:UT
AS-79-1840-P
PJV- GA
8-17-79

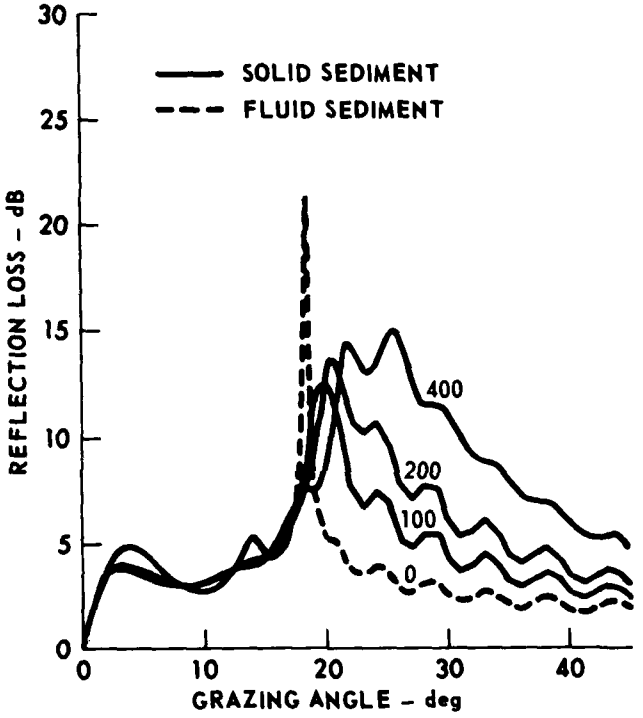

FIGURE 33
REFLECTION LOSS versus GRAZING ANGLE
FOR A 100 m THICK CLAY LAYER AT 100 Hz
THE PARAMETER IS THE SEDIMENT SHEAR
WAVE SPEED IN UNITS OF m/sec

ARL:UT
AS-79-1841-P
PJV - GA
8 - 17 - 79

At 25 Hz (Fig. 31) and 50 Hz (Fig. 32), a small increase in the shear speed (v_2 = 100 m/sec) greatly increases the energy loss to the interface wave. Increasing the S wave velocity further shifts the peak location to higher angles. The peak is both broadened and reduced in magnitude. At v_2 = 400 m/sec the peak at 25 Hz can still be distinguished although it is now very broad. At 50 Hz the peak can no longer be unambiguously identified but appears as part of the set of P wave interference peaks. A general increase in RL above about 17° is seen for all values of S wave speed. This is expected since the location of the Stoneley wave (v_2=0) in angle occurs very near the critical angle below which the P wave interaction with the substrate is negligible. For larger angles sediment S waves are excited at the substrate interface and RL is increased.

At 100 Hz (Fig. 33) the energy loss to interface waves does not greatly increase for v_2 = 100 m/sec. Rather, the interface wave peak is broadened and lowered in magnitude. For v_2 = 200 m/sec and 400 m/sec the existence of an interface wave peak in RL cannot be clearly observed. The RL shows the expected increase due to sediment S wave excitation in angles above about 18°.

One possible explanation for the results in Figs. 31-33 follows. The main effect of sediment S waves for small S wave velocities (100 m/sec) at low frequencies is to add a significant energy loss mechanism through the relatively large S wave absorption. This greatly increases the RL and results in the large peaks in Figs. 31 and 32. At higher frequencies (Fig. 33) the loss to sediment P wave and substrate P and S wave absorption is large enough to produce the large RL in the absence of sediment S waves and thus the effect of more absorption is not important. At all frequencies the effect of increasing S wave velocity is to broaden and decrease the magnitude of the interface wave peak until it merges with the general increase in RL due to sediment S wave excitation.

A more realistic layer structure would include a shear speed gradient. The additional effects of a constant gradient of 3 sec^{-1} is shown in Figs. 34-36. This gradient approximates that expected in deep sea marine sediments. The surficial shear speed was taken to be 100 m/sec, giving a value at the substrate interface of 400 m/sec. For comparison, RL for the fluid sediment and the solid sediment with v_2 = 400 m/sec and no shear speed gradient are also shown.

As seen in Figs. 34-36, the addition of an S wave velocity gradient appears to make no qualitative change in the effect of sediment rigidity on energy lost to interface waves. The shape and magnitude of the RL for a homogeneous layer (dotted curve) fairly well approximates that of the layer with a gradient. This is expected since both sediment structures have the same S wave speed at the substrate interface. The major effect appears to be a shift in the location of the P wave oscillation in RL.

Sediment parameters typical of sands, important in shallow water continental shelf environments, have not been specifically treated in the present paper. Sands differ from clays in two acoustically important ways. First, the sound velocity in sands is higher than that in water (1780 m/sec at the sediment surface compared to 1540 m/sec in water). This means that the P wave is evanescent in sands. Specular reflection from the water interface is more efficient than in clays. This combines with the exponentially decaying evanescent wave to determine the P wave amplitude at the substrate interface. Secondly, the gradients of parameters in the first few meters are substantially larger than in clays. The P wave velocity gradient, for example, can be about 20 sec^{-1} in sands compared to 2 sec^{-1} in clays.[22] These large near-surface gradients raise the possibility that gradient driven P-S coupling may be an important mechanism for exciting S waves in sands at low frequencies. This process is explicitly neglected in our computational model.[15] If, in fact, this additional excitation mechanism is negligible, our analysis procedure could be extended to treat sand sediment types.

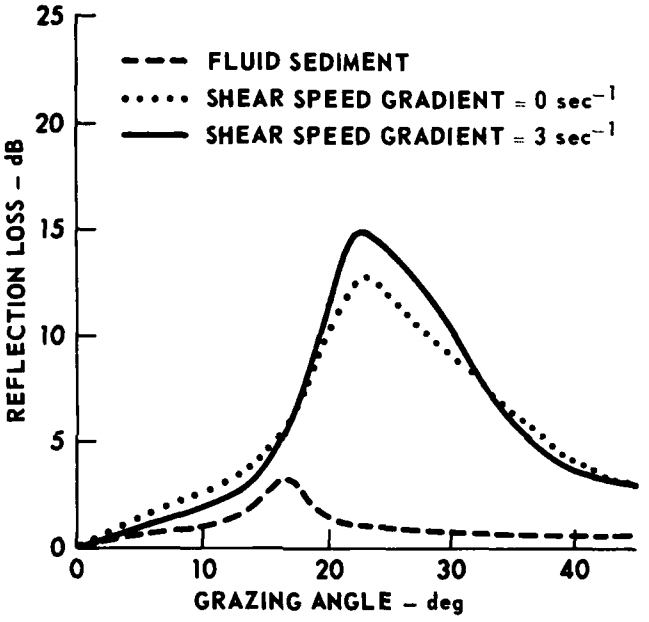

FIGURE 34
REFLECTION LOSS versus GRAZING ANGLE
FOR A 100 m THICK CLAY LAYER AT 25 Hz
THE SEDIMENT SHEAR SPEED AT THE
SUBSTRATE IS 400 m/sec

ARL:UT
AS-79-1842-P
PJV - GA
8 - 17 - 79

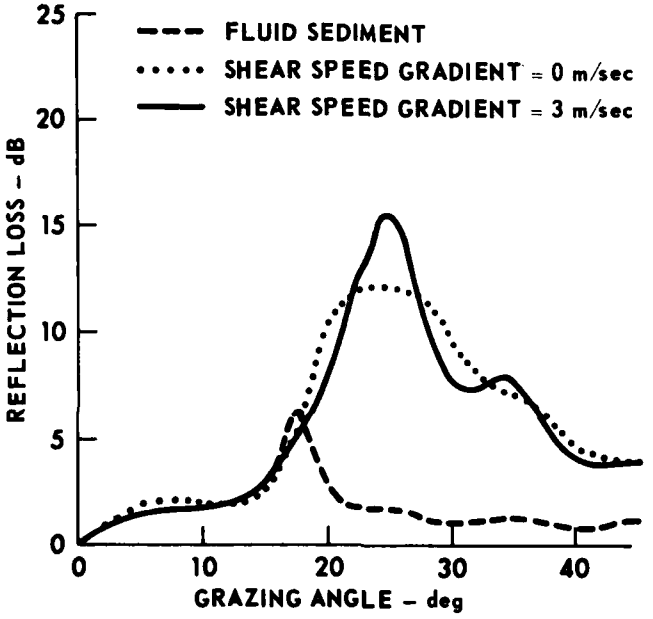

FIGURE 35
REFLECTION LOSS versus GRAZING ANGLE
FOR A 100 m THICK CLAY LAYER AT 50 Hz
THE SEDIMENT SHEAR SPEED AT THE
SUBSTRATE IS 400 m/sec

ARL:UT
AS-79-1843-P
PJV-GA
8-17-79

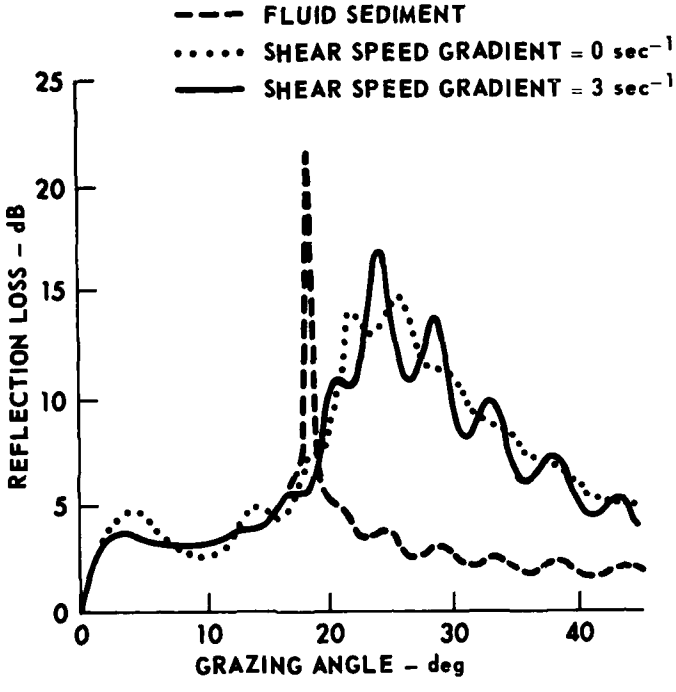

FIGURE 36
REFLECTION LOSS versus GRAZING ANGLE
FOR A 100 m THICK CLAY LAYER AT 100 Hz
THE SEDIMENT SHEAR SPEED AT THE
SUBSTRATE IS 400 m/sec

ARL:UT
AS-79-1844-P
PJV - GA
8 - 17 - 79

V. SUMMARY

A study of the effect of sediment rigidity on bottom reflection loss (RL) from typical deep sea sediment types shows that sediment shear (S) wave excitation is important for thin sediment layers but is negligible for thick layers. The major mechanism for S wave excitation is compressional (P) wave conversion at the sediment-substrate interface. Little energy is coupled into S waves at the water-sediment interface.

The mechanism for S wave excitation provides a means for quantifying the categories of thick and thin layers. It is the P wave amplitude at the substrate interface that is important. If the P wave amplitude at the substrate interface is significant, the layer is ~~thick~~ thin; if it is small, the layer is ~~thin~~ thick. In general there is a grazing angle θ_o separating a low angle region, in which the P wave turning point is well above the substrate, from a high angle region, in which the P wave strikes the substrate interface, or has a turning point near the interface. For angles less than θ_o the layer is thick and S wave effects are negligible. For angles greater than θ_o the layer is thin and S wave effects produce significant increases in RL. For physically thick layers, θ_o is large and S wave effects are negligible for all grazing angles, except for a shift in the peak structure between the critical angles for substrate S and P wave propagation. For physically thin layers, θ_o can be 0° and sediment rigidity will be particularly important at low grazing angles.

For thin layers the dependence of RL on frequency shows the existence of high and low frequency regimes. The total attenuation of the S wave traveling one way through the sediment provides a means for separating these frequency regimes. For total S wave attenuation greater than 20 dB, an S wave generated at the substrate interface is effectively

absorbed within the sediment without striking the other interface. Since we assume attenuation is proportional to frequency, this defines a "high" frequency regime in which the propagation of sediment S waves can be neglected; however their excitation is still an important loss mechanism. At "low" frequencies, S wave attenuation is less than 20 dB across the layer and the additional interference effects due to the propagation of S waves through the sediment are important. Very large peaks in RL (>20 dB) are possible.

A theoretical treatment of the reflection and transmission coefficients at the water and substrate interfaces by means of an expansion in the small sediment S wave velocity provides a basis for developing a ray picture of the effects of sediment rigidity on RL. The basic mechanism for S wave excitation emerges as P wave conversion at the substrate interface. The dependence on S wave velocity and attenuation and P wave attenuation are predicted by the ray picture. The interference structure is found to be due to the interference of a wave similar to that generated in a fluid sediment, the A_o wave, and waves whose amplitudes depend on the S wave velocity to the first power, the A_1 wave, and to the second power, the A_2 wave. The parameter dependencies predicted by the ray picture are verified in detail by results obtained from the computational model.

Parameter studies, with ranges of variation restricted by geophysical data, are used to identify significant parameters in determining RL in solid sediments. The results obtained agree, in general, with the results expected from the ray picture. Important sediment properties are found to be density, P and S wave velocities, and the gradients of P and S wave velocities. These must be specified to better than half their geophysically allowable range in order to obtain RL to within 1 dB. Just as important, some negligible parameters were also identified. These include the gradients of sediment density P and S wave velocity gradients, all attenuations except the sediment S wave attenuation, and the substrate density. These parameters may take on any value within their geophysical range without changing the reflection coefficient by 10%. The remaining parameters can be important under some conditions and negligible in others.

Also presented were the results of parameter studies which indicate the accuracy required in specifying geoacoustic parameters. Parameters typical of a deep sea sediment layer were varied by ±10%. The resulting changes in RL were used to identify parameter sensitivity. RL from solid sediments was found to be particularly sensitive to water sound speed, sediment thickness, density, and compressional wave speed, and to substrate shear velocity. Very low sensitivity parameters are all attenuations and their gradients, and the gradients of sediment density and P wave velocity. Other parameters produced fractional changes in the reflection coefficient of the same size as the fractional change in the parameter.

Sediment rigidity was also found to influence the energy lost to interface waves. The Stoneley wave, generated in the fluid sediment case, merges into generally increased RL in solid sediments, and the peak in RL at a particular grazing angle, characteristic of interface waves, cannot be identified in solid sediments with realistic geophysical parameters.

In summary, a computational model of the bottom reflection loss of a solid sediment layer was used to study the effect of sediment rigidity on bottom reflection loss. For thin sediment layers compressional wave conversion at the substrate interface is the dominant mechanism for the excitation of sediment shear waves. Significant increases in bottom reflection loss are possible at fairly high frequencies (hundreds of hertz). For low frequencies the effects of sediment rigidity can dominate the reflection loss. For thick sediment layers the compressional wave conversion cannot take place at the substrate interface because the wave is refracted relatively high in the sediment. In this case the effects of sediment rigidity are negligible. A ray picture of the acoustic processes was developed and used to understand and interpret the results of the computational model. Parameter studies are reported which identify important bottom parameters in determining the reflection loss

in solid sediments. The influence of parameter accuracy in predicting bottom reflection loss is treated using parameter studies. For realistic bottom parameters the loss of energy to interface waves does not appear to be an important, distinct process, as in the case of a fluid sediment.

ACKNOWLEDGMENTS

The author has greatly benefited from numerous discussions with K. E. Hawker, S. R. Rutherford, C. Tindle, C. W. Horton, Sr., T. L. Foreman, and E. L. Hamilton. This work was supported by Naval Ocean Research and Development Activity and Naval Electronic Systems Command.

REFERENCES

1. S. R. Rutherford and K. E. Hawker, "The Effects of Density Gradients on Bottom Reflection Loss for a Class of Marine Sediments," J. Acoust. Soc. Am. 63, 750-757 (1978).

2. K. E. Hawker et al., "A Sensitivity Study of Underwater Sound Propagation Loss and Bottom Loss," Applied Research Laboratories Technical Report No. 77-17 (ARL-TR-77-17), Applied Research Laboratories, The University of Texas at Austin (1977).

3. A. O. Williams, Jr., "Hidden Depths: Acceptable Ignorance about Ocean Bottoms," J. Acoust. Soc. Am. 59, 1175-1179 (1976).

4. K. E. Hawker, W. E. Williams, and T. L. Foreman, "A Study of the Acoustical Effects of Subbottom Absorption Profiles," J. Acoust. Soc. Am. 65, 360-367 (1979).

5. K. E. Hawker, "The Influence of Stoneley Waves on Plane Wave Reflection Coefficients: Characteristics of Bottom Reflection Loss," J. Acoust. Soc. Am. 64, 548-555 (1978).

6. K. E. Hawker, "Existence of Stoneley Waves as a Loss Mechanism in Plane Wave Reflection Problems," J. Acoust. Soc. Am. 65, 682-686 (1979).

7. S. R. Rutherford et al., "A Study of the Effects of Ocean Bottom Roughness on Low-Frequency Sound Propagation," J. Acoust. Soc. Am. 65, 381-386 (1979).

8. H. P. Bucker, J. A. Whitney, G. S. Yee, and R. R. Gardner, "Reflection of Low-Frequency Sonar Signals from a Smooth Ocean Bottom," J. Acoust. Soc. Am. 37, 1037-1051 (1965).

9. G. J. Fryer, "Reflectivity of the Ocean Bottom at Low Frequency," J. Acoust. Soc. Am. 63, 35-42 (1978).

10. E. L. Hamilton, "Shear-Wave Velocity versus Depth in Marine Sediments: A Review," Geophys. 41, 985-996 (1976).

11. E. L. Hamilton, "Attenuation of Shear Waves in Marine Sediments," J. Acoust. Soc. Am. 60, 334-338 (1976).

12. D. J. Shirley and L. D. Hampton, "Shear Wave Measurements in Laboratory Sediments," J. Acoust. Soc. Am. 63, 607-613 (1978).

13. P. J. Vidmar and T. L. Foreman, "The Effect of Sediment Rigidity on the Acoustic Reflectivity of the Ocean Bottom," EOS, Trans. Am. Geophys. Union 59, 1119(A) (1978).

14. P. J. Vidmar and T. L. Foreman, "A Plane-Wave Reflection Loss Model Including Sediment Rigidity," J. Acoust. Soc. Am. 65, S43(A) (1979).

15. P. J. Vidmar and T. L. Foreman, "A Plane-Wave Reflection Loss Model Including Sediment Rigidity," accepted for publication in The Journal of The Acoustical Society of America.

16. L. M. Brekhovskikh, Waves in Layered Media (Academic Press, New York, 1960).

17. Our coordinate system differs from that in Ref. 16 by a parity transformation. Our z axis increases downward, while that in Ref. 16 increases upward. This results in the difference in sign between our Eq. (19) and the result in Ref. 16.

18. E. L. Hamilton, "Sound Attenuation as a Function of Depth in the Sea Floor," J. Acoust. Soc. Am. 59, 528-535 (1976).

19. E. L. Hamilton, "Prediction of Deep-Sea Sediment Properties: State-of-the-Art," in Deep-Sea Sediments, Physical and Mechanical Properties, edited by A. L. Inderbitzen (Plenum Press, New York, 1974).

20. E. L. Hamilton, "Variations of Density and Porosity with Depth in Deep-Sea Sediments," J. Sediment. Petrol. 46, 280-300 (1976).

21. E. L. Hamilton, "Sound Velocity-Density Relations in Sea-Floor Sediments and Rocks," J. Acoust. Soc. Am. 63, 366-377 (1978).

22. E. L. Hamilton, "Sound Velocity Gradients in Marine Sediments," J. Acoust. Soc. Am. 65, 909-922 (1979).

19 September 1979

DISTRIBUTION LIST FOR
ARL-TR-79-49
UNDER CONTRACT N00014-78-C-0113

Copy No.

Commanding Officer
Naval Ocean Research and Development Activity
NSTL Station, MS 39529
1 Attn: CDR J. Paquin (Code 500)
2 R. Martin (Code 115)
3 S. W. Marshall (Code 340)
4 H. Eppert (Code 360)
5 A. L. Anderson (Code 320)
6 M. G. Lewis (Code 500)
7 J. Matthews (Code 360)
8 G. Morris (Code 340)
9 R. R. Goodman (Code 110)

Commanding Officer
Office of Naval Research
Arlington, VA 22217
10 Attn: A. Sykes (Code 222)
11 T. Pyle (Code 483)
12 H. Bezdek (Code 480T)
13 M. McKisic (Code 486)
14 R. S. Andrews (Code 463)
15 M. Odegard (Code 483)

16 Office of Naval Research
Branch Office, Chicago
Department of the Navy
536 South Clark Street
Chicago, IL 60605

Commanding Officer
Naval Electronic Systems Command
Washington, DC 20360
17 Attn: J. Sinsky (Code 320)
18 C. R. Rollins (Code 320)
19 CDR D. Griffiths (Code 320)
20 Code PME 124-30
21 Code PME 124-62
22 Code PME 124TA

Distribution List for ARL-TR-79-49 under Contract N00014-78-C-0113 (Cont'd)

Copy No.

42 Commander
Naval Surface Weapons Center
White Oak Laboratory
Department of the Navy
Silver Spring, MD 20910

43 Commander
David W. Taylor Naval Ship Research and
Development Center
Department of the Navy
Bethesda, MD 20034

Naval Oceanographic Office
NSTL Station, MS 39529
44 Attn: W. Jobst (Code 3440)
45 W. H. Geddes

Commander
Naval Air Development Center
Department of the Navy
Warminister, PA 18974
46 Attn: P. Van Schuyler (Code 2052)
47 C. L. Bartberger
48 P. Haas

Officer in Charge
New London Laboratory
Naval Underwater Systems Center
Department of the Navy
New London, CT 06320
49 Attn: F. R. DiNapoli
50 R. Deavenport
51 J. Papadakis
52 R. Lauer
53 P. Herstein
54 R. Hasse

55 Assistant Director
Ocean Control DDR & E
Room 3D, 1048 Pentagon
Washington, DC 20301

OASN (R, E & S)
Room 4D, 745 Pentagon
Washington, DC 20301
56 Attn: G. A. Cann

AD-A079 661 TEXAS UNIV AT AUSTIN APPLIED RESEARCH LABS F/G 20/1
THE EFFECT OF SEDIMENT RIGIDITY ON BOTTOM REFLECTION LOSS.(U)
SEP 79 P J VIDMAR N00014-78-C-0113
UNCLASSIFIED ARL-TR-79-49 NL

2 OF 2
AD A079661

END
DATE FILMED
2-80
DDC

Distribution List for ARL-TR-79-49 under Contract N00014-78-C-0113 (Cont'd)

Copy No.

Defense Advanced Research Projects Agency
Acoustic Research Center
Moffett Field, CA 94035
57 Attn: E. Smith

Defense Advanced Research Projects Agency
1400 Wilson Boulevard
Arlington, VA 22209
58 Attn: T. Kooij

Superintendent
Naval Postgraduate School
Monterey, CA 93940
59 Attn: Library
60 H. Medwin
61 O. B. Wilson

Commanding Officer
Naval Air Systems Command
Department of the Navy
Washington, DC 20361
62 Attn: CDR J. Messegee (Code PMA-264)

Commander
Naval Coastal Systems Center
Department of the Navy
Panama City, FL 32407
63 Attn: G. McLeroy

64 - 75 Commanding Officer and Director
Defense Documentation Center
Cameron Station, Building 5
5010 Duke Street
Alexandria, VA 22314

Arthur D. Little, Inc.
15 Acorn Park
Cambridge, MA 02140
76 Attn: G. Raisbeck

Woods Hole Oceanographic Institution
86-95 Water Street
Woods Hole, MA 02543
77 Attn: E. E. Hayes
78 G. Frisk
79 R. Spindel
80 B. Tucholke

Distribution List for ARL-TR-79-49 under Contract N00014-78-C-0113 (Cont'd)

Copy No.

Science Applications, Inc.
8400 Westpark Drive
McLean, VA 22101
81 Attn: J. Hanna
82 C. Spofford
83 L. Dozier

Applied Research Laboratory
The Pennsylvania State University
P.O. Box 30
State College, PA 16801
84 Attn: S. McDaniel

Underwater Systems, Inc.
World Building
8121 Georgia Avenue
Silver Spring, MD 20910
85 Attn: M. S. Weinstein

Marine Physical Laboratory of
The Scripps Institution of Oceanography
The University of California, San Diego
San Diego, CA 92132
86 Attn: V. Anderson
87 F. Fisher
88 G. Shor

Scripps Institution of Oceanography
The University of California, San Diego
La Jolla, CA 92037
89 Attn: Library
90 R. Tyce
91 J. Orcutt
92 L. Dorman

Tracor, Inc.
1601 Research Boulevard
Rockville, MD 20850
93 Attn: J. Gottwald
94 A. Wittenborn
95 R. J. Urick

Bell Telephone Laboratories, Inc.
Whippany Road
Whippany, NJ 07961
96 Attn: S. A. Kramer
97 F. Labianca

Copy No.

Planning Systems, Inc.
7900 Westpark Drive, Suite 507
McLean, VA 22101
98 Attn: L. Solomon
99 R. Cavanaugh

TRW, Inc.
TRW Defense & Space Systems Group
Washington Operations
7600 Colshire Drive
McLean, VA 22101
100 Attn: R. T. Brown
101 I. Gereben

SUTRON Corporation
Suite 700
1925 North Lynn Street
Arlington, VA 22209
102 Attn: C. Dabney

Daubin Systems Corporation
104 Crandon Boulevard
Key Biscayne, FL 33149
103 Attn: S. Daubin

Defence Scientific Establishment
HMNZ Dockyard
Devonport, Auckland
NEW ZEALAND
104 Attn: K. M. Guthrie
105 R. N. Denham
106 R. Bannister

Physics Department
The University of Auckland
Private Bag, Auckland
NEW ZEALAND
107 Attn: A. C. Kibblewhite
108 G. Bold
109 C. T. Tindle

The Catholic University of America
Washington, DC 20064
110 Attn: H. M. Uberall

Distribution List for ARL-TR-79-49 under Contract N00014-78-C-0113 (Cont'd)

Copy No.

Department of Geology and Geophysics
Geophysical and Polar Research Center
Lewis G. Weeks Hall for Geological Sciences
The University of Wisconsin, Madison
1215 W. Dayton Street
Madison, WI 53706
111 Attn: C. S. Clay

Courant Institute
251 Mercer Street
New York, NY 10012
112 Attn: D. C. Stickler

Bolt, Beranek, and Newman, Inc.
50 Moulton Street
Cambridge, MA 02138
113 Attn: P. W. Smith, Jr.

Boeing Aerospace Corporation
Advanced Projects
P.O. Box 3999, M.S. 84-63
Seattle, WA 98124
114 Attn: Bob Arnold

The Institute of Acoustic Research
615 SW 2nd Avenue
Miami, FL 33130
115 Attn: N. Kronengold
116 J. Clark
117 R. Flanagan

Department of Ocean Engineering
Massachusetts Institute of Technology
Cambridge, MA 02139
118 Attn: Professor I. Dyer

Hawaii Institute of Geophysics
The University of Hawaii
2525 Correa Road
Honolulu, HI 96822
119 Attn: G. Sutton
120 G. Fryer
121 M. Manghnani

Distribution List for ARL-TR-79-49 under Contract N00014-78-C-0113 (Cont'd)

Copy No.

Director
North Atlantic Treaty Organization
SACLANT ASW Research Centre
APO New York 09019
122 Attn: T. Akal
123 F. Jensen
124 D. Ross
125 W. Kuperman

Defence Research Establishment Pacific
CF Dockyard
Victoria, B.C.
CANADA
126 Attn: G. R. Ebbeson

Defence Research Establishment Atlantic
9 Grove Street
P.O. Box 1012
Dartmouth, N.S.
CANADA
127 Attn: I. Fraser
128 D. Chapman

Rosenteil School of Marine and
Atmospheric Science
The University of Miami
10 Rickenbacker Causeway
Miami, FL 33149
129 Attn: Dr. H. DeFerrari

Applied Physics Laboratory
The Johns Hopkins University
Johns Hopkins Road
Laurel, MD 20810
130 Attn: L. H. Wallman

Polar Research Laboratory, Inc.
123 Santa Barbara Street
Santa Barbara, CA 93101
131 Attn: B. M. Buck

The University of Miami
10 Rickenbacker Causeway
Miami, FL 33149
132 Attn: Dr. F. Tappert

Distribution List for ARL-TR-79-49 under Contract N00014-78-C-0113 (Cont'd)

Copy No.

Physics Department
The University of Rhode Island
Kingston, RI 02881
133 Attn: C. Kaufman

Department of Electrical Engineering
Polytechnic Institute of New York
Farmingdale, NY 11735
134 Attn: L. B. Folsen

135 I. Tolstoy
Knockvennie, Castle Douglas
S.W. SCOTLAND
GREAT BRITAIN

National Oceanic and Atmospheric Administration
Environmental Research Laboratories
Boulder, CO 80303
136 Attn: J. R. Wait

Geophysics Laboratory
Marine Science Institute
The University of Texas
700 The Strand
Galveston, TX 77550
137 Attn: J. Worzel

Department of Electrical Engineering
The University of Texas at Austin
Austin, TX 78712
138 Attn: Francis X. Bostick
139 Dr. E. Hixon

Department of Geology
The University of Texas at Austin
Austin, TX 78712
140 Attn: Dr. M. M. Backus
141 Dr. Clark Wilson

School of Mechanical Engineering
Georgia Institute of Technology
Atlanta, GA 30332
142 Attn: Dr. A. D. Pierce

Distribution List ARL-TR-79-49 under Contract N00014-78-C-0113 (Cont'd)

Copy No.

Brown University
Providence, RI 02912
143 Attn: A. O. Williams, Jr.

The Lamont-Doherty Geological Observatory
Columbia University
Palisades, NY 10964
144 Attn: R. D. Stoll
145 H. A. Kutschale
146 R. E. Houtz

147 Office of Naval Research
Resident Representative
Room No. 582, Federal Bldg.
Austin, TX 78701

148 Glen E. Ellis, ARL:UT

149 Terry L. Foreman, ARL:UT

150 Ruth Gonzales, ARL:UT

151 Loyd D. Hampton, ARL:UT

152 Kenneth E. Hawker, ARL:UT

153 John J. Lemmon, ARL:UT

154 Stephen K. Mitchell, ARL:UT

155 Susan G. Payne, ARL:UT

156 Steven R. Rutherford, ARL:UT

157 Jack A. Shooter, ARL:UT

158 Clark S. Penrod, ARL:UT

159 Dana S. Hougland, ARL:UT

160 Paul, J. Vidmar, ARL:UT

161 Reuben H. Wallace, ARL:UT

162 Claude W. Horton, Sr., ARL:UT

163 Garland R. Barnard, ARL:UT

164 Library, ARL:UT

165 - 195 Reserve, ARL:UT